

Isotopic geochemistry, zircon U–Pb ages and Hf isotopes of A-type granites from the Xitian W–Sn deposit, SE China: Constraints on petrogenesis and tectonic significance



Yun Zhou ^{a,b}, Xinquan Liang ^{a,*}, Shichong Wu ^c, Yongfeng Cai ^b, Xirong Liang ^a, Tongbin Shao ^d, Ce Wang ^a, Jiangang Fu ^a, Ying Jiang ^a

^a State Key Laboratory of Isotope Geochemistry, Guangzhou Institute of Geochemistry, Chinese Academy of Sciences, Guangzhou 510640, China

^b College of Earth Sciences, Guilin University of Technology, Guilin 541004, China

^c 416 Geological Team, Bureau of Geology and Mineral Exploration and Development of Hunan Province, Zhuzhou 412007, China

^d Département des Génies Civil, Géologique et des Mines, École Polytechnique de Montréal, C.P. 6079, succursale Centre-ville, Montréal, Québec H3C 3A7, Canada

ARTICLE INFO

Article history:

Received 6 October 2014

Received in revised form 3 March 2015

Accepted 5 March 2015

Available online 17 March 2015

Keywords:

Geochemistry

Zircon U–Pb dating

A-type granite

W–Sn deposit

Southeast China

ABSTRACT

Zircon U–Pb geochronological, geochemical and petrological analyses have been carried out on the Xitian granite emplaced in the middle part of Shi-Hang zone, which is closely related to the economically important Xitian tungsten–tin deposit in Hunan Province, Southeast China. LA-ICP-MS zircon U–Pb dating of two representative samples yielded weighted means $^{206}\text{Pb}/^{238}\text{U}$ age of 151.7 ± 1.2 Ma and 151.8 ± 1.4 Ma. These granites are comprised mainly of K-feldspar, quartz, plagioclase, Fe-rich biotite and minor fluorite, and are characterized by enrichments in Rb, Th, REEs (total REE = 159–351 ppm), and HFSEs (e.g., Zr and Y) but depletions in Ba, Sr, P, Eu and Ti. They are metaluminous to weakly peraluminous and show a clear A-type granite geochemical signature with high SiO_2 (73.44–78.45 wt.%), total alkalis ($\text{Na}_2\text{O} + \text{K}_2\text{O} = 2.89\text{--}8.98$ wt.%), $\text{Fe}_2\text{O}_3^*/\text{MgO}$ ratios and low P_2O_5 , CaO , MgO and TiO_2 contents. In-situ zircon Hf isotope analysis suggests their $\varepsilon_{\text{Hf}}(t)$ values ranging from −7.43 to −14.69. Sr–Nd isotope data show their $\varepsilon_{\text{Nd}}(t)$ values in the range of −9.2 to −7.3, with corresponding T_{DM2} ages of 1.72–1.56 Ga. These characteristics indicate that the Xitian granite originated from partial melting of metamorphic basement rocks with a certain amount of mantle-derived materials. Combined with previous geochemical and isotopic data, it is derived that mantle–crust interaction was gradually enhanced from the early to late stages of magmatism. The ore-forming materials and fluids of the Xitian W–Sn deposit are mainly produced by the Early Yanshanian granitic magmatism, which is also responsible for the Late Jurassic (ca. 152 Ma) A-type granitic rocks that host the W–Sn polymetallic deposits distributed along the Shi-Hang zone, implying a significant Mesozoic extensional event in Southeast China likely caused by the subduction of the Paleo-Pacific plate.

© 2015 Elsevier Ltd. All rights reserved.

1. Introduction

South China Block (SCB) was formed by the amalgamation between Cathaysia and Yangtze Blocks at ca. 1.0–0.9 Ga during the assembly of Neoproterozoic Rodinia supercontinent (Li and McCulloch, 1996; Li et al., 2007b, 2009; Ye et al., 2007). In Mesozoic era, the SCB was geologically characterized by widespread igneous rocks which consist predominantly of granites and rhyolites and subordinate mafic intrusive and volcanic rocks

(Li et al., 2007a). A large number of geochemical, petrological and tectonic analyses were performed on these igneous in the past decades, but geodynamic background and tectonic setting in which they were generated have been a topic of debate (e.g. Faure and Natalin, 1992; Lapierre et al., 1997; Martin et al., 1994; Zhang, 2013; Zhou and Li, 2000). It is widely accepted that the active continental margin of eastern Asia is related to the subduction of the Paleo-Pacific plate beneath the Eurasia plate (e.g. Jahn et al., 1976; Lapierre et al., 1997; Martin et al., 1994). An alternative intraplate extension and/or rifting regime caused by super mantle plume (Zhang, 2013; Zhang et al., 2009) or collision between the Indochina and South China blocks during Early Mesozoic (Gilder et al., 1991) has been proposed to account for the development of subordinate rifting-related alkaline basalts and syenites (Li

* Corresponding author at: Guangzhou Institute of Geochemistry, Chinese Academy of Sciences, Wushan, Guangzhou 510640, Guangdong Province, China. Tel.: +86 20 85290113.

E-mail address: liangxq@gig.ac.cn (X. Liang).

et al., 2004a; Wang et al., 2004a), bimodal volcanic and intrusive rocks (Chen et al., 1999; Wang et al., 2005), and mafic dykes in SE China hinterland (Li and McCulloch, 1998). In addition, a flat-slab subduction and slab-foundering model has been proposed by Li et al. (2007a) to interpret the development of the broad Mesozoic magmatic province in the SCB.

The Late-Mesozoic Xitian granites were exposed at the south-central of "Shi-Hang zone" which was proposed by Gilder et al. (1996) for a granitic belt with relative higher $\varepsilon_{\text{Nd}}(t)$ values and younger $T_{\text{DM}2}$ of Nd model ages from Hangzhou City (Zhejiang Province) through central Jiangxi and southern Hunan Provinces to Shiwandashan (Guangxi Province) in South China (Fig. 1). Due to their close relationship with the giant Xitian W-Sn polymetallic deposit, Xitian granites have received a number of studies, most of which focused on the geological characteristics, prospecting potential and ore-controlling factors of the Xitian skarn tin-polymetallic orefield (Fu et al., 2012; Liu et al., 2008; Wu et al., 2012; Zhou et al., 2013). However, detailed petrogenesis and geodynamic setting of the granites, which are important to ore-forming potential evaluation, are not well understood. In this study, we present new geochronological, petrological and geochemical data for the Xitian granites, and combine them with previous data in order to (1) discuss their petrogenetic characteristics, (2) constrain their geodynamic background, and (3) explore the relationship between granitic magmatism and tungsten-tin mineralization.

2. Geological setting

The SCB is bordered by the North China Craton through the Qinling-Dabie-Sulu orogenic belt to the north, the Three River orogenic belts and the Songpan-Gantze Block to the west, the Indochina Block through Red River-Ailaoshan Fault to the southwest, and the Philippine Sea Plate in the east. The SCB consists of the Yangtze Block in the northwest and the Cathaysia Block in the southeast. The southeastern margin of the SCB used to be considered as a passive margin until Late Paleozoic to Early Mesozoic when the Pale-Pacific plate was subducted beneath the SCB along the Taiwan-Mariana Islands (Hsü et al., 1990; Li et al., 2006a, 2012). A large number of Late Mesozoic volcanic-intrusive complexes were exposed in SE China from the Early to Late Yanshanian in three major episodes: 180–160 Ma, 160–135 Ma and 135–90 Ma (Zhou and Li, 2000; Li et al., 2010a; Jiang and Li, 2014). Different types of granitoids including I-, A- and S-type granites during Late Mesozoic were generated, and the A-type granites mainly distributed along the regional and local fault zones (Wong et al., 2009).

Abundant Cretaceous-Tertiary NE-trending red-bed basins such as the Shiwandashan basin and Gan-Hang basin emerged concurrently with the latest phase of the regional magmatic activity, and consist mainly of red-colored clastic rocks and basalt interlayer (Gilder et al., 1996; Fig. 1). Bimodal volcanic activity took

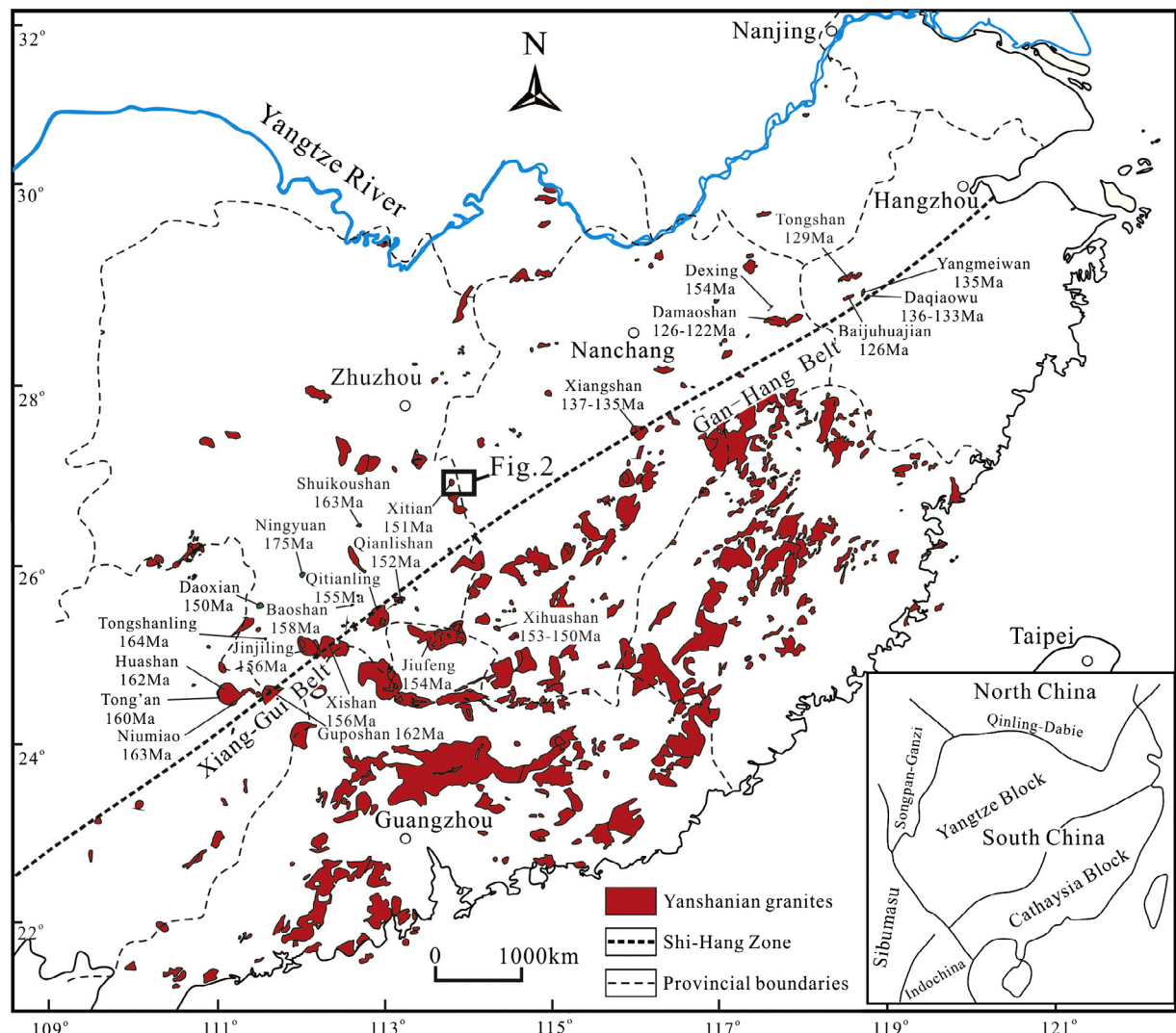


Fig. 1. Schematic geological map showing distribution of Mesozoic granitoids (modified after Zhou et al., 2006). The cited geochronological data are from Table 7.

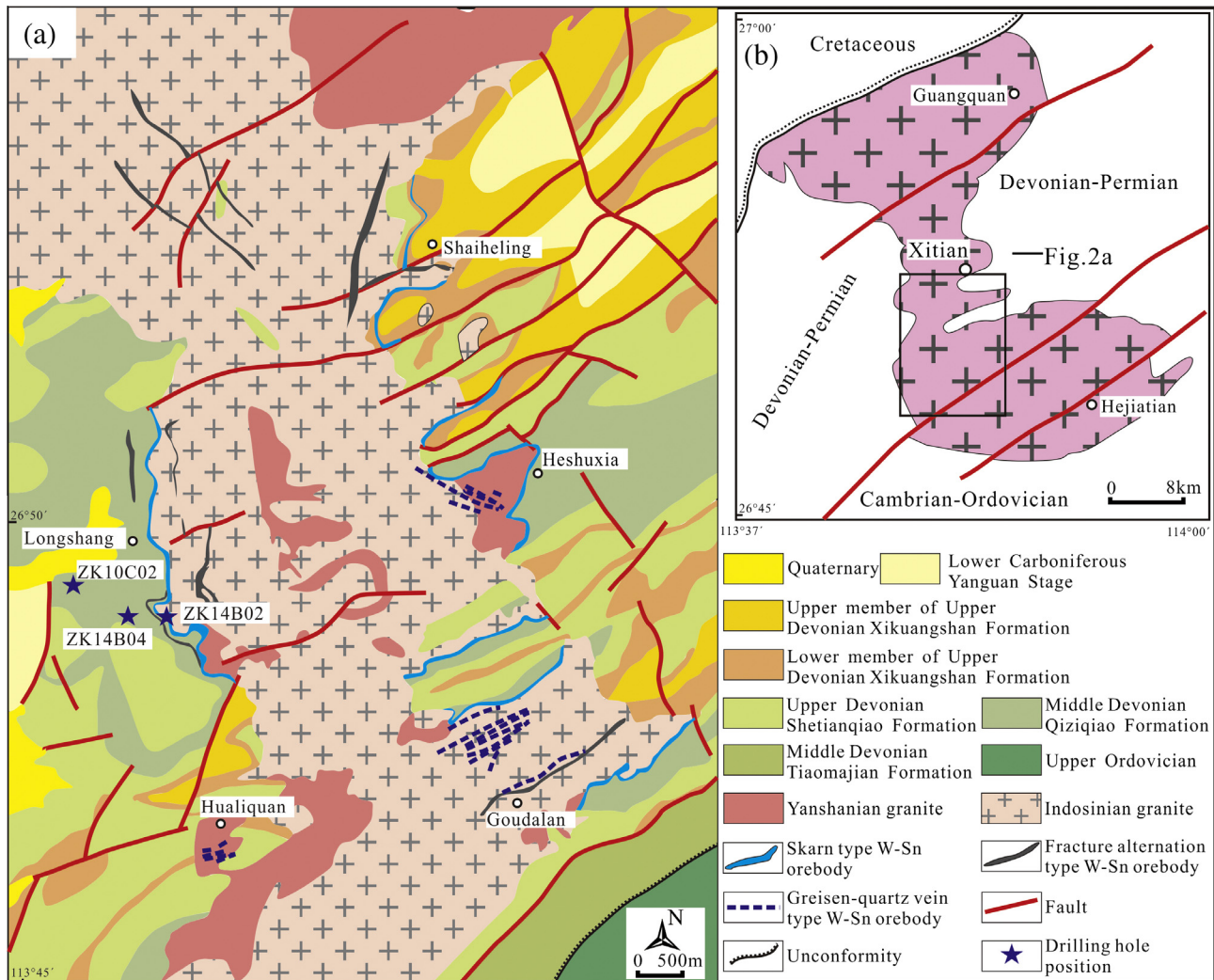


Fig. 2. The simplified geological map of the Xitian W-Sn polymetallic deposit.

place in the Gan-Hang basin during the Early Cretaceous, and plentiful granite porphyry dikes intruded into the Early Cretaceous red-bed basins (Jiang et al., 2006). The basaltic rocks with average thickness around 10 m are interbedded with the Early Cretaceous red mudstone. Gilder et al. (1996) called this NNE-trending zone of extensional basins as the “Shi-Hang zone”, and divided it into the south part in the southern Hunan-northern Guangxi provinces (named as Xiang-Gui Belt) and the north part in western Zhejiang-eastern Jiangxi provinces (called as Gan-Hang Belt) (Fig. 1). The Xiang-Gui Belt contains lots of granitic complexes such as the Qianlishan, Qitianling, Xishan, Jinjiling, Huashan, Guposhan and Kunlunshan granites, while the Gan-Hang Belt includes the Doushui, Shangyou, Yanbei, Zudong, Xiangshan, Dexing, Lingshan granites, etc. (Fig. 1; Chen and Jahn, 1998; Chen et al., 1999). The granites in this zone are high in Sm ($>8 \times 10^{-6}$), Nd ($>45 \times 10^{-6}$) and $\epsilon_{\text{Nd}}(t)$ values (>-8), but low in T_{DM} model ages (<1.5 Ga) and initial $^{87}\text{Sr}/^{86}\text{Sr}$ values (<0.710), and they were dated mainly from 164 to 151 Ma (Zhou et al., 2013).

Xitian is located in Zhuzhou City, Hunan Province, Southeast China (Fig. 1). Xitian granites are located in the geographical intersection of Hunan and Jiangxi Provinces and belong to the Xiang-Gui Belt. Tectonically, they lie on the borderline between the Yangtze and Cathaysia Blocks, and extend in NE-direction along the southern side of the Chenzhou-Linwu ultracrustal fault. The Xitian granites intruded into Devonian strata with an outcrop area

of ca. 230 km², and the surrounding rock is composed of skarn, chert, schist and slate with width of 300–1200 m. The Xitian granitic batholith consists of Indosinian granites (γ_5^1), Early Yanshanian granites (γ_5^2) and Late Yanshanian granites (γ_5^3). The Indosinian granites have the largest outcrop area and distribute as batholith or stock. The Early Yanshanian granites were exposed scarcely on the surface, but connected with each other below the surface and intruded into the Indosinian granites as stock or apophysis. A few Late Yanshanian granites intruded into the surface and exist as boss and apophysis.

3. Sampling and petrography

Among the Xitian granitic batholith, the Indosinian granite is composed mainly of fine- to medium-grained porphyritic biotite monzonitic granite with granitic texture and massive structure. They are characterized by 10–15% phenocrysts consisting of almost K-feldspar and matrixes containing 30–35% quartz, 30–40% K-feldspar, 25–30% plagioclase, 3–9% biotite and ca. 0.2% fluorite. Accessory minerals are magnetite, ilmenite, tourmaline, apatite and zircon. The Early Yanshanian granite is made up largely of fine-grained porphyritic biotite monzogranites and has porphyritic or granitic texture and massive structure. The phenocrysts (ca. 5%) are K-feldspar and the matrixes comprise 28–30% quartz, 28–38%

K-feldspar, 25–30% plagioclase, 5–12% biotite, and minor muscovite (<1%) and fluorite (<0.1%). Accessory minerals involve magnetite, tourmaline, apatite, topaz and zircon. The major rock type of the Late Yanshanian granite is fine-grained two-mica granite with granitic texture and massive structure, and consists of 35–40% quartz, 30–36% K-feldspar, 20–25% plagioclase, 3–5% muscovite, 2–3% biotite, ca. 2% topaz, and minor zoisite (ca. 0.1%) and fluorite (<0.1%). Accessory minerals contain magnetite, apatite and zircon.

Forty-three samples of Early Yanshanian granite, including 36 samples of fine- to medium-grained granite and 7 of coarse-grained granite were collected from the Xitian deposit (Fig. 2). All the samples are gray, and most of them are fresh or only weakly altered, as observed from hand specimens and under the microscope, and all of them were crushed for chemical analyses. Among these samples, two representative samples (ZK10C02-13 and ZK14B04-02) were chosen for in situ zircon U-Pb dating and thirty were cut for thin sections. The granite samples in this study have massive structure and porphyrae texture with ca. 5% phenocryst consisted dominantly of K-feldspar with 0.001–4.5 mm in size (Fig. 3). The matrixes contain 25–35% K-feldspar, 20–35% plagioclase, 20–30% quartz, 5–10% biotite and ca. 1% muscovite. The biotites exhibit high Fe/(Fe + Mg) ratios and thus belong to siderophyllite (Table 1 and Fig. 4). Accessory minerals are composed of magnetite, tourmaline, apatite and zircon. Local sericitization of plagioclase and intrusion of quartz veins into the granitic host rocks can be observed (Fig. 3), probably resulted from late-stage of hydrothermal activity.

4. Analytical methods

4.1. Mineral composition analyses

Mineral composition and back-scattered-electron image analyses on biotite were carried out at the State Key Laboratory of Isotope Geochemistry, Guangzhou Institute of Geochemistry,

Chinese Academy of Sciences (SKLIG GIG CAS) with a JEOL JXA-8100 Superprobe. Operating conditions were as follows: 15 kV accelerating voltage, 20 nA beam current, 1–2 μm beam diameter, 10 s counting time and ZAF correction procedure for data reduction. The analytical procedures were similar to those described by Huang et al. (2007).

4.2. Zircon U-Pb geochronology and Hf isotopic composition

Representative samples ZK10C02-13 and ZK14B04-02, which are from the borehole ZK10C02 and ZK14B04, respectively, were selected for zircon U-Pb dating and Hf isotopic measurement. Zircon grains were separated from crushed rock samples by conventional magnetic and heavy liquid separation, and then hand-picked under a binocular microscope. Randomly selected zircon grains were mounted on adhesive tape, then enclosed in epoxy resin and polished to section the crystals in about half for analysis. The transmitted and reflected light as well as cathodoluminescence (CL) images were taken of the zircon grains to reveal their internal structure and morphology and select spots for U-Pb dating analysis. CL images for the zircon grains analyzed were performed at the Scanning Electron Microscope (SEM) of Institute of Geology and Geophysics, Chinese Academy of Sciences. U-Pb dating was conducted by LA-ICP-MS at the SKLIG GIG CAS. LA-ICP-MS laser ablation sampling adopted the approach of single point erosion. Fragments of the standard TEM zircon grains (TEMORA 1, 417 Ma; Black et al., 2003) were incorporated in each mount as reference to correct for inter-element fractionation. Zircon Temora was chosen as the standards in zircon U-Pb dating and in U and Th content correction. Trace-element concentrations were obtained by normalizing count rates for each analyzed element to those for Si, and assuming SiO_2 to be stoichiometric in zircon (Tu et al., 2011). In order to ensure the reliability of the measured results and then to monitor the stability of the instrument, the standard sample Temora should be measured twice after every five

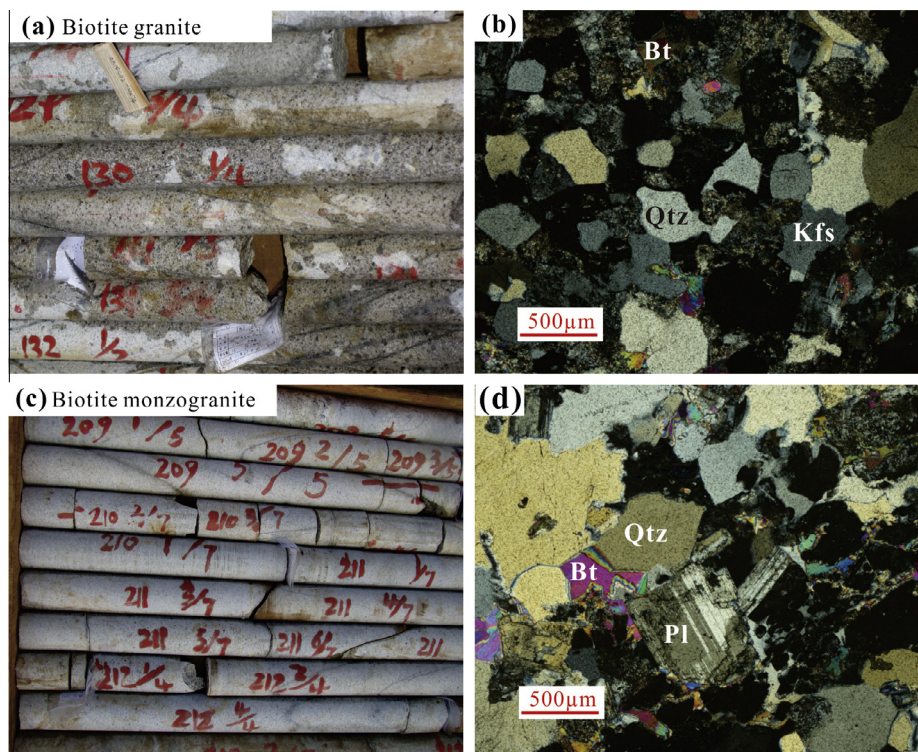


Fig. 3. Drill hole samples (a) biotite granite and (b) biotite monzogranite, and (c), (d) show the photomicrographs of representative samples from Xitian granite. Kfs: K-feldspar. Pl: plagioclase. Qtz: quartz. Bt: biotite.

Table 1

Representative electron microprobe analytical results of biotite from Xitian granite (wt.%).

Sample	SiO ₂	TiO ₂	Al ₂ O ₃	FeO	Fe ₂ O ₃	MnO	MgO	CaO	Na ₂ O	K ₂ O	Cr ₂ O ₃	Total	Si	AlIV	AlVI	Ti	Fe3	Fe2	Mn	Mg	Ca	Na	K	Cr	Fe/(Fe + Mg)	Mg/(Fe + Mg)
ZK10C02-20-1	46.47	0.409	26.97	7.80	1.18	0.491	0.650	—	0.168	9.77	—	93.78	6.81	1.19	3.47	0.045	0.130	0.957	0.061	0.142	0	0.048	1.828	0	0.87	0.13
ZK10C02-20-2	42.05	0.550	21.75	13.74	1.92	0.706	0.761	0.007	0.142	9.84	0.06	91.34	6.66	1.34	2.71	0.065	0.229	1.820	0.095	0.180	0.001	0.044	1.988	0.008	0.91	0.09
ZK10C02-20-3	40.41	1.090	21.19	15.91	2.14	0.717	0.938	—	0.125	9.76	0.011	92.07	6.45	1.55	2.44	0.131	0.257	2.124	0.097	0.223	0	0.039	1.989	0.001	0.90	0.10
ZK10C02-20-4	40.22	0.926	21.34	16.70	2.21	0.688	1.218	0.061	0.153	9.71	—	93.00	6.39	1.61	2.38	0.111	0.264	2.218	0.093	0.288	0.01	0.047	1.966	0	0.89	0.11
ZK10C02-20-5	39.60	1.487	21.02	17.78	2.31	0.771	1.217	0.063	0.074	9.72	0.016	93.83	6.29	1.72	2.21	0.178	0.276	2.360	0.104	0.288	0.011	0.023	1.969	0.002	0.89	0.11
ZK10C02-20-6	44.78	0.455	25.98	9.97	1.47	0.476	1.078	—	0.208	9.85	0.021	94.13	6.66	1.34	3.21	0.051	0.164	1.239	0.060	0.239	0	0.060	1.867	0.002	0.84	0.16
ZK10C02-30-1	43.04	0.517	25.04	12.38	1.77	0.952	0.132	—	0.113	10.14	0.007	93.92	6.55	1.45	3.04	0.059	0.203	1.576	0.123	0.030	0	0.033	1.970	0.001	0.98	0.02
ZK10C02-30-2	44.70	0.296	27.04	10.19	1.50	0.715	0.186	0.009	0.197	10.20	—	94.88	6.61	1.39	3.32	0.033	0.167	1.261	0.090	0.041	0.001	0.057	1.925	0	0.97	0.03
ZK10C02-30-3	38.50	0.857	22.69	18.13	2.33	1.141	0.201	0.045	0.186	9.65	0.077	93.57	6.15	1.85	2.42	0.103	0.279	2.423	0.154	0.048	0.008	0.058	1.967	0.01	0.98	0.02
ZK10C02-30-4	46.02	0.195	27.82	8.40	1.26	0.681	0.128	—	0.191	10.45	0.042	95.06	6.72	1.29	3.50	0.021	0.138	1.025	0.084	0.028	0	0.054	1.944	0.005	0.97	0.03
ZK10C02-33-1	46.08	0.276	25.62	10.37	1.53	0.767	0.181	0.026	0.145	10.34	0.021	95.18	6.80	1.21	3.24	0.031	0.169	1.279	0.096	0.040	0.004	0.041	1.945	0.002	0.97	0.03
ZK10C02-33-2	45.42	0.331	26.06	9.85	1.46	0.731	0.189	0.024	0.152	10.08	0.016	94.16	6.75	1.25	3.31	0.037	0.163	1.224	0.092	0.042	0.004	0.044	1.910	0.002	0.97	0.03
ZK10C02-33-3	45.96	0.231	27.72	8.00	1.20	0.242	0.262	—	0.194	10.33	—	94.02	6.75	1.25	3.54	0.026	0.133	0.981	0.030	0.057	0	0.055	1.934	0	0.95	0.05
ZK10C02-33-4	43.01	0.525	26.06	9.47	1.40	0.608	0.302	0.081	0.269	10.02	—	91.60	6.59	1.41	3.30	0.061	0.161	1.213	0.079	0.069	0.013	0.080	1.958	0	0.95	0.05
ZK14B04-02-1	46.45	0.314	25.87	9.52	1.41	0.614	0.558	—	0.122	10.35	—	95.07	6.82	1.19	3.29	0.035	0.156	1.169	0.076	0.122	0	0.035	1.938	0	0.91	0.09
ZK14B04-02-2	47.44	0.137	28.34	7.33	1.11	0.367	0.577	—	0.111	10.77	0.045	96.10	6.79	1.21	3.56	0.015	0.119	0.876	0.044	0.123	0	0.031	1.965	0.005	0.88	0.12
ZK14B04-02-3	46.26	0.071	26.68	9.49	1.41	0.633	0.598	—	0.109	10.35	0.005	95.46	6.76	1.24	3.35	0.008	0.154	1.159	0.078	0.130	0	0.031	1.928	0.001	0.90	0.10
ZK14B04-02-4	48.94	0.340	29.41	5.96	0.91	0.317	0.517	—	0.112	10.71	—	97.12	6.85	1.15	3.69	0.036	0.096	0.698	0.038	0.108	0	0.030	1.911	0	0.87	0.13
ZK14B04-12-1	37.93	0.214	22.32	20.02	2.46	0.808	0.134	0.062	0.073	9.61	0.016	93.39	6.13	1.87	2.38	0.026	0.298	2.706	0.111	0.032	0.011	0.023	1.980	0.002	0.99	0.01
ZK14B04-12-2	39.63	0.174	23.02	20.35	2.54	0.810	0.166	—	0.070	9.73	—	96.23	6.19	1.81	2.42	0.020	0.298	2.657	0.107	0.039	0	0.021	1.938	0	0.99	0.01
ZK14B04-12-3	40.16	0.359	23.53	18.82	2.42	0.803	0.159	—	0.132	9.95	0.02	96.11	6.23	1.77	2.52	0.042	0.282	2.440	0.105	0.037	0	0.040	1.968	0.002	0.99	0.01
ZK14B04-12-4	39.78	0.413	22.96	19.44	2.47	0.739	0.120	—	0.145	9.81	0.02	95.64	6.22	1.78	2.45	0.049	0.290	2.542	0.098	0.028	0	0.044	1.957	0.002	0.99	0.01
ZK15001-1-1	37.27	1.120	20.44	23.83	2.62	1.131	0.433	—	0.154	9.47	0.011	96.22	5.99	2.01	1.86	0.135	0.317	3.204	0.154	0.104	0	0.048	1.943	0.001	0.97	0.03
ZK15001-1-2	37.61	1.269	20.90	23.91	2.66	1.085	0.432	—	0.055	9.64	0.038	97.33	5.97	2.03	1.88	0.152	0.318	3.174	0.146	0.102	0	0.017	1.953	0.005	0.97	0.03
ZK15001-1-3	36.75	1.500	20.86	24.98	2.66	1.119	0.390	—	0.122	9.42	0.042	97.57	5.86	2.14	1.78	0.180	0.319	3.331	0.151	0.093	0	0.038	1.917	0.005	0.97	0.03
ZK15001-1-4	36.53	1.426	20.72	24.80	2.67	1.130	0.424	—	0.116	9.13	0.042	96.72	5.87	2.13	1.79	0.172	0.323	3.332	0.154	0.102	0	0.036	1.871	0.005	0.97	0.03
ZK55A02-1-1	50.11	0.162	26.76	3.15	0.49	0.021	4.565	0.01	0.119	10.66	—	96.00	7.00	1.00	3.40	0.017	0.051	0.368	0.002	0.950	0.001	0.032	1.899	0	0.28	0.72
ZK55A02-1-2	48.86	0.455	26.63	3.49	0.54	0.006	5.271	0.002	0.165	10.49	0.064	95.92	6.86	1.14	3.26	0.048	0.057	0.409	0.001	1.103	0	0.045	1.879	0.007	0.27	0.73
ZK55A02-1-3	50.29	0.168	28.57	2.48	0.39	0.175	3.989	—	0.056	10.17	—	96.24	6.95	1.05	3.60	0.017	0.040	0.286	0.020	0.822	0	0.015	1.792	0	0.26	0.74
ZK55A02-1-4	49.23	0.210	27.65	3.12	0.49	0.084	4.180	0.001	0.107	10.63	0.005	95.65	6.90	1.10	3.47	0.022	0.051	0.365	0.010	0.874	0	0.029	1.901	0.001	0.29	0.71

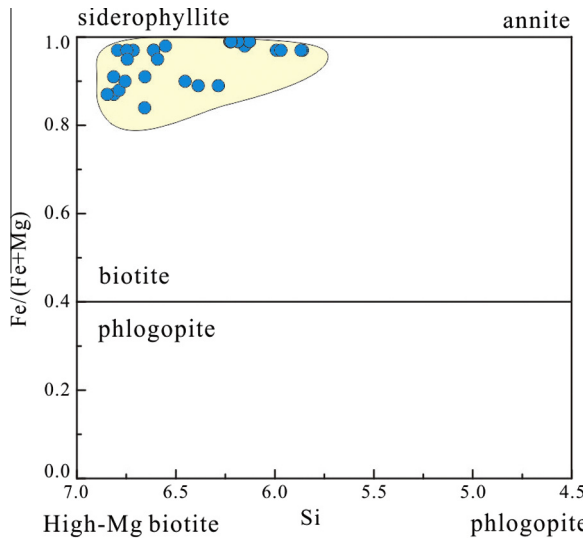


Fig. 4. Chemical classification diagram of biotite (after Eby and Kochhar, 1990).

points. Pb isotopic data, U-Pb ages and U-Th contents of the zircons analysis-spots were processed with the help of ICPMSDataCal (Liu et al., 2010). Common Pb correction was applied using the method of Andersen (2002) by assuming zero-age Pb loss, which has negligible effect on the age results. Detailed analytical data in which individual analyses are shown with 1σ error and uncertainties in weighted mean ages are quoted at the 95% confidence level (2σ) are given in Table 2. Concordia diagrams and weighted mean calculations were made using Isoplot/Ex_ver3 (Ludwig, 2001).

In situ zircon Hf isotopic measurements on the sample ZK14B04-02 were performed on a Neptune Plus multi-collection inductively coupled plasma mass spectrometry. Details of Hf isotopic analytical method followed Wu et al. (2006). Normalizing factor used to correct the mass fractionation of Hf during the measurements is 0.7325 for $^{179}\text{Hf}/^{177}\text{Hf}$. The reference value of $^{176}\text{Hf}/^{177}\text{Hf}$ of standard Penglai Zircon is 0.282906 ± 0.000010 (2s) (Li et al., 2010c). Analyses of standard Penglai zircon over the measurement period provided $^{176}\text{Hf}/^{177}\text{Hf} = 0.282926 \pm 0.000016$ (2s) ($n = 6$). Initial $^{176}\text{Hf}/^{177}\text{Hf}$ values were calculated based on Lu decay constant of $1.865E-11$ (Scherer et al., 2001). The model ages were

Table 2
LA-ICP-MS zircon U-Pb isotopic analyses of the representative Xitian granite.

Spot	^{232}Th (ppm)	^{238}U (ppm)	Th/U	$^{207}\text{Pb}/^{206}\text{Pb}$		$^{207}\text{Pb}/^{235}\text{U}$		$^{206}\text{Pb}/^{238}\text{U}$		$^{207}\text{Pb}/^{206}\text{Pb}$		$^{207}\text{Pb}/^{235}\text{U}$		$^{206}\text{Pb}/^{238}\text{U}$	
				Ratios	σ	Ratios	σ	Ratios	σ	Age (Ma)	σ	Age (Ma)	σ	Age (Ma)	σ
<i>ZK10C02-13(113°45'35"E, 26°49'28"N)</i>															
1.1	300	717	0.42	0.0501	0.0061	0.1588	0.0138	0.0237	0.0005	198	259	150	12	151	3
2.1	365	848	0.43	0.0539	0.0044	0.1699	0.0143	0.0242	0.0004	369	185	159	12	154	3
3.1	283	510	0.56	0.0482	0.0035	0.1473	0.0146	0.0236	0.0006	109	167	146	10	151	4
4.1	334	557	0.6	0.0466	0.0044	0.1556	0.0137	0.0237	0.0005	33	206	147	12	151	3
5.1	257	467	0.55	0.0469	0.0047	0.1538	0.0150	0.0236	0.0005	56	278	145	13	150	3
6.1	327	575	0.57	0.0517	0.0035	0.1636	0.0118	0.0237	0.0004	272	156	154	10	151	3
7.1	209	399	0.52	0.0516	0.0055	0.1650	0.0174	0.0238	0.0004	333	49	155	15	151	2
8.1	272	479	0.57	0.0506	0.0045	0.1704	0.0151	0.0240	0.0005	220	6	160	13	153	3
9.1	785	2155	0.36	0.0508	0.0036	0.1636	0.0127	0.0240	0.0008	232	165	154	11	153	5
10.1	244	454	0.54	0.0474	0.0047	0.1543	0.0148	0.0234	0.0005	78	222	146	13	149	3
11.1	192	354	0.54	0.0520	0.0077	0.1655	0.0245	0.0238	0.0008	283	307	155	21	152	5
12.1	1092	5124	0.21	0.0464	0.0032	0.1539	0.0137	0.0236	0.0008	20	169	145	12	150	5
13.1	289	519	0.56	0.0509	0.0041	0.1664	0.0146	0.0236	0.0005	239	187	156	13	150	3
14.1	222	421	0.53	0.0472	0.0044	0.1501	0.0140	0.0237	0.0005	61	272	142	12	151	3
15.1	255	621	0.41	0.0477	0.0029	0.1572	0.0132	0.0242	0.0005	87	146	148	12	154	3
16.1	211	378	0.56	0.0483	0.0045	0.1549	0.0143	0.0238	0.0005	122	198	146	13	152	3
17.1	281	494	0.57	0.0469	0.0067	0.1536	0.0225	0.0235	0.0005	43	311	145	20	150	3
18.1	230	420	0.55	0.0508	0.0044	0.1641	0.0133	0.0236	0.0005	235	193	154	12	150	3
19.1	1257	7047	0.18	0.0499	0.0020	0.1404	0.0151	0.0243	0.0003	191	90	133	13	155	2
20.1	221	420	0.53	0.0470	0.0042	0.1555	0.0141	0.0237	0.0005	50	200	147	12	151	3
21.1	371	766	0.48	0.0503	0.0034	0.1626	0.0106	0.0236	0.0005	209	156	153	9	151	3
22.1	259	468	0.55	0.0489	0.0053	0.1564	0.0161	0.0236	0.0006	146	237	148	14	150	4
23.1	230	432	0.53	0.0506	0.0052	0.1582	0.0158	0.0239	0.0005	233	222	149	14	152	3
<i>ZK14B04-02(113°45'51"E, 26°49'17"N)</i>															
1.1	303	658	0.46	0.0477	0.0029	0.1550	0.0097	0.0235	0.0004	87	146	146	9	149	2
2.1	480	875	0.55	0.0467	0.0023	0.1515	0.0078	0.0235	0.0004	32	119	143	7	150	2
3.1	287	566	0.51	0.0465	0.0047	0.1587	0.0182	0.0244	0.0005	33	217	150	16	155	3
4.1	345	1273	0.27	0.0475	0.0027	0.1549	0.0085	0.0235	0.0005	76	135	146	8	150	3
5.1	383	837	0.46	0.0461	0.0036	0.1563	0.0120	0.0242	0.0004	400	-217	147	11	154	3
6.1	325	713	0.46	0.0473	0.0037	0.1552	0.0116	0.0237	0.0005	65	174	146	10	151	3
7.1	155	291	0.53	0.0467	0.0052	0.1592	0.0187	0.0241	0.0005	35	248	150	16	153	3
8.1	175	335	0.52	0.0482	0.0035	0.1611	0.0124	0.0239	0.0005	109	167	152	11	152	3
9.1	363	716	0.51	0.0515	0.0036	0.1738	0.0123	0.0244	0.0004	261	158	163	11	155	3
10.1	208	378	0.55	0.0524	0.0050	0.1740	0.0155	0.0244	0.0005	302	214	163	13	155	3
11.1	192	255	0.75	0.0522	0.0059	0.1666	0.0182	0.0235	0.0005	295	257	156	16	150	3
12.1	387	483	0.80	0.0510	0.0039	0.1661	0.0127	0.0237	0.0005	243	178	156	11	151	3
13.1	143	205	0.70	0.0475	0.0065	0.1537	0.0235	0.0237	0.0006	76	296	145	21	151	4
14.1	236	509	0.46	0.0498	0.0035	0.1646	0.0120	0.0238	0.0005	187	165	155	11	152	3
15.1	97	180	0.54	0.0501	0.0061	0.1558	0.0179	0.0239	0.0006	198	259	147	16	152	4
16.1	237	747	0.32	0.0461	0.0030	0.1557	0.0119	0.0237	0.0004	400	-250	147	10	151	3
17.1	91	162	0.56	0.0506	0.0089	0.1560	0.0247	0.0230	0.0008	220	363	147	22	149	3

Table 3

Zircon Hf isotope analyses for the Xitian granite.

Grain no.	$^{176}\text{Yb}/^{177}\text{Hf}$	2s	$^{176}\text{Lu}/^{177}\text{Hf}$	2s	$^{176}\text{Hf}/^{177}\text{Hf}$	2s	$^{176}\text{Hf}/^{177}\text{Hf}_{\text{fi}}$	$\varepsilon_{\text{Hf}}(t)$	2σ	T_{DM1} (Ma)	T_{DM2} (Ma)	$f_{\text{Lu/Hf}}$
<i>ZK14B04-02 (113°45'51"E, 26°49'17"N)</i>												
1.1	0.025492	0.000082	0.000657	0.000003	0.282452	0.000015	0.282450	-8.11	0.53	1122	1371	-0.98
5.1	0.047723	0.001950	0.001229	0.000054	0.282436	0.000017	0.282432	-8.63	0.60	1162	1401	-0.96
6.1	0.031403	0.000442	0.000874	0.000006	0.282462	0.000017	0.282460	-7.73	0.60	1114	1354	-0.97
7.1	0.027740	0.000549	0.000752	0.000020	0.282461	0.000017	0.282459	-7.70	0.59	1112	1354	-0.98
8.1	0.029599	0.000691	0.000830	0.000030	0.282444	0.000024	0.282442	-8.33	0.85	1138	1385	-0.97
9.1	0.048912	0.000645	0.001259	0.000030	0.282438	0.000018	0.282434	-8.54	0.64	1160	1397	-0.96
10.1	0.030425	0.000450	0.000846	0.000023	0.282370	0.000021	0.282367	-10.92	0.72	1243	1514	-0.97
11.1	0.032385	0.001098	0.000864	0.000030	0.282471	0.000019	0.282469	-7.43	0.68	1101	1338	-0.97
12.1	0.054171	0.000576	0.001463	0.000029	0.282448	0.000020	0.282444	-8.30	0.68	1152	1382	-0.96
13.1	0.035361	0.000309	0.000895	0.000013	0.282444	0.000015	0.282442	-8.36	0.53	1140	1385	-0.97
14.1	0.052787	0.001871	0.001385	0.000057	0.282400	0.000021	0.282396	-9.97	0.72	1217	1464	-0.96
15.1	0.027140	0.000553	0.000791	0.000023	0.282368	0.000036	0.282366	-11.02	1.27	1242	1516	-0.98
16.1	0.032559	0.000326	0.000951	0.000015	0.282266	0.000035	0.282263	-14.69	1.22	1391	1695	-0.97
17.1	0.022403	0.000163	0.000604	0.000008	0.282460	0.000013	0.282458	-7.83	0.47	1109	1357	-0.98

Table 4

Major element contents (%) of Xitian granite.

Sample	SiO_2	TiO_2	Al_2O_3	Fe_2O_3	MnO	MgO	CaO	Na_2O	K_2O	P_2O_5	LOI	Total
ZK10C02-01	74.39	0.03	13.72	0.69	0.04	0.42	1.93	0.27	3.54	0.01	4.67	99.72
ZK10C02-02	78.45	0.10	12.84	1.61	0.06	0.28	0.33	0.01	2.87	0.02	3.00	99.57
ZK10C02-03	74.27	0.10	12.81	2.07	0.10	0.11	1.45	0.14	5.87	0.02	2.59	99.53
ZK10C02-04	73.44	0.09	12.64	1.66	0.08	0.19	0.85	3.48	5.49	0.02	1.57	99.50
ZK10C02-05	74.98	0.09	12.86	1.59	0.09	0.14	0.88	2.09	5.28	0.02	1.48	99.50
ZK10C02-06	75.41	0.11	12.48	1.78	0.09	0.23	0.83	1.39	5.21	0.02	1.96	99.51
ZK10C02-07	75.84	0.10	12.88	1.52	0.07	0.17	0.94	0.10	5.55	0.02	2.35	99.54
ZK10C02-08	76.29	0.12	12.41	1.76	0.06	0.16	0.85	0.12	5.67	0.02	2.03	99.49
ZK10C02-09	75.21	0.10	12.59	1.71	0.06	0.20	1.23	0.11	5.61	0.02	2.71	99.53
ZK10C02-10	75.18	0.04	13.33	0.92	0.04	0.20	0.57	2.36	5.18	0.01	1.67	99.50
ZK10C02-11	75.98	0.14	11.20	1.83	0.08	<0.001	0.86	3.19	5.22	0.03	1.20	99.71
ZK10C02-12	74.90	0.13	12.70	1.87	0.08	0.13	0.81	2.34	5.12	0.02	1.38	99.48
ZK10C02-13	76.37	0.11	12.94	1.62	0.06	0.38	0.57	0.05	5.23	0.02	2.17	99.51
ZK10C02-14	75.08	0.11	12.72	1.53	0.05	0.05	0.74	3.10	5.07	0.02	0.99	99.46
ZK10C02-15	74.29	0.12	12.49	1.66	0.05	0.09	0.81	3.93	4.91	0.02	1.11	99.48
ZK10C02-16	75.41	0.12	12.59	1.70	0.05	0.06	0.84	3.12	4.63	0.02	0.94	99.48
ZK10C02-17	74.64	0.12	13.08	1.63	0.05	0.07	0.75	2.93	5.25	0.02	0.94	99.48
ZK10C02-18	75.88	0.10	12.38	1.56	0.05	0.05	0.78	2.96	4.74	0.02	0.96	99.48
ZK10C02-19	75.31	0.12	12.78	1.58	0.05	0.09	0.80	2.85	4.84	0.02	1.04	99.48
ZK10C02-20	75.22	0.13	12.52	1.81	0.06	0.14	0.86	2.42	4.92	0.02	1.37	99.48
ZK10C02-21	74.97	0.14	12.59	1.66	0.05	0.42	0.96	2.49	5.16	0.01	1.29	99.48
ZK10C02-22	75.76	0.15	13.09	1.48	0.05	0.28	0.86	0.16	5.04	0.02	2.75	99.55
ZK10C02-23	77.51	0.15	12.00	1.41	0.04	0.11	0.92	0.06	4.83	0.02	2.42	99.53
ZK10C02-24	75.37	0.16	12.40	1.75	0.04	0.19	0.92	2.66	4.88	0.02	1.12	99.48
ZK10C02-25	76.95	0.19	13.57	1.23	0.03	0.14	0.25	0.07	3.88	0.02	3.07	99.54
ZK10C02-26	75.53	0.17	13.90	0.96	0.02	0.23	0.84	0.06	4.48	0.02	3.32	99.57
ZK10C02-27	74.54	0.06	13.48	1.57	0.05	0.18	0.91	0.15	5.07	0.02	3.34	99.56
ZK10C02-28	78.39	0.04	12.82	0.97	0.03	0.16	0.77	0.02	3.93	0.02	2.34	99.53
ZK10C02-29	73.58	0.05	13.56	1.16	0.04	0.20	0.82	1.90	5.67	0.02	2.37	99.52
ZK10C02-30	73.54	0.06	12.84	1.39	0.08	0.20	2.22	0.10	5.85	0.01	3.28	99.57
ZK10C02-31	74.98	0.06	13.13	1.21	0.05	<0.001	0.88	3.23	4.78	0.03	1.11	99.48
ZK10C02-32	74.83	0.05	12.86	1.47	0.05	0.13	0.70	4.24	4.24	0.02	1.02	99.49
ZK10C02-33	76.12	0.05	12.56	1.35	0.05	0.38	0.70	2.97	4.71	0.02	0.94	99.47
ZK10C02-34	76.09	0.04	12.92	1.01	0.03	0.05	0.67	3.97	4.04	0.02	0.69	99.48
ZK10C02-35	75.58	0.05	12.68	1.13	0.04	0.09	0.71	3.42	4.39	0.02	1.47	99.48
ZK10C02-36	76.68	0.09	12.35	1.44	0.04	0.06	0.82	2.04	4.95	0.02	0.88	99.47
ZK14B04-02	74.93	0.10	12.52	1.87	0.06	0.17	0.86	2.36	5.00	0.03	1.61	99.51
ZK14B04-05	75.20	0.12	12.74	1.64	0.04	0.06	0.79	2.92	5.15	0.02	0.79	99.47
ZK14B04-07	75.51	0.07	12.90	1.09	0.03	0.03	0.65	2.87	5.53	0.02	0.78	99.47
ZK14B04-09	76.68	0.08	12.23	1.31	0.03	0.07	0.66	2.84	4.60	0.02	0.95	99.48
ZK14B04-12	73.96	0.03	13.84	1.29	0.02	0.13	0.88	3.91	4.19	0.02	1.21	99.48
ZK14B02-01	74.69	0.12	12.87	1.40	0.04	0.21	0.91	2.48	5.24	0.02	1.50	99.48
ZK14B02-03	76.38	0.13	12.33	1.25	0.04	0.11	1.06	0.72	5.49	0.03	1.98	99.51

computed under the assumption that the $^{176}\text{Lu}/^{177}\text{Hf}$ of average crust is 0.015, and the $^{176}\text{Hf}/^{177}\text{Hf}$ and $^{176}\text{Lu}/^{177}\text{Hf}$ ratios of chondrite and depleted mantle at the present are, respectively, 0.282772 and 0.0332, and 0.28325 and 0.0384 (BlichertToft and Albarede, 1997). The analytical results of Hf isotopic compositions are listed in Table 3.

4.3. Major and trace element analyses

Major and trace element analyses were carried out on representative samples collected from the Xitian composite granite. Selected relatively fresh rocks were first split into small chips and ultrasonically cleaned in distilled water, then crushed to very

Table 5
Trace element concentrations (ppm) of Xitian granite.

Sample	ZK10C02-01	ZK10C02-03	ZK10C02-07	ZK10C02-12	ZK10C02-15	ZK10C02-17	ZK10C02-19	ZK10C02-20	ZK10C02-22	ZK10C02-25	ZK10C02-27	ZK10C02-30	ZK10C02-33	ZK10C02-36	ZK14B04-02	ZK14B04-07	ZK14B04-12	ZK14B02-01
Sc	8.4	9.2	7.8	8.1	8.3	8.3	9.0	8.5	8.4	8.1	9.9	8.7	8.9	9.0	9.6	8.0	10.8	8.5
Ti	65.2	411	431	602	585	506	565	596	681	882	234	234	190	184.3	422.4	294.1	37	535.8
V	21.6	32.0	25.9	26.9	27.3	20.5	24.3	30.0	26.3	27.9	18.7	25.4	24.3	23.1	28.5	25.7	24.6	25.4
Cr	162	260	180	191	186	154	179	233	167	161	176	210	214	205	233	207	197	187
Mn	335	836	585	591	416	435	398	444	368	199	381	681	426	325	470	235	180	275
Co	0.60	1.47	0.98	1.35	1.25	1.08	1.15	1.40	1.23	1.28	0.73	0.99	1.01	0.95	1.26	0.91	0.90	1.09
Ni	10.76	13.59	11.78	12.21	12.39	10.90	11.72	13.16	11.53	11.26	11.06	14.01	12.66	11.86	13.07	12.67	12.74	11.9
Cu	19.2	61.0	139	145	19.3	40.0	12.9	203	63.8	6.2	2.98	123	177	126	11.8	6.4	7.4	3.8
Zn	15.3	438	254	676	101.3	92.9	50.7	89.8	119	39.8	31.9	47.7	63.9	37.3	44.8	33.3	24.8	28.7
Ga	16.1	15.6	14.9	14.1	14.5	15.1	14.9	14.3	15.0	15.2	17.7	16.2	15.6	15.4	16.8	16.0	20.7	16.5
Ge	2.16	2.72	2.78	3.45	2.72	2.88	2.69	2.83	2.36	2.21	2.19	2.43	2.72	2.70	2.78	2.46	3.06	2.23
Rb	572	1083	940	904	793	852	814	801	833	662	1070	1119	946	825	882	790	682	727
Sr	26.9	23.5	10.8	14.6	13.0	11.2	11.2	15.1	12.0	14.7	10.9	20.7	6.7	7.0	16.3	14.1	13.5	21.4
Y	121	94.8	70.5	77.7	81.9	97.4	106	98.1	74.8	78.9	140	147	139	193	128	116	37.1	88.1
Zr	88.7	145	120	136	176	132	159	158	211	219	86.2	132	105	116	139	86.8	38.4	155
Nb	24.4	26.5	29.43	28.4	29.0	29.5	34.7	28.5	28.5	30.1	46.2	38.0	30.3	45.8	24.7	23.7	52.5	30.4
Cs	56.0	67.4	67.5	69.2	73.1	70.9	67.7	64.8	70.6	66.4	91.3	69.6	46.5	36.2	61.9	43.2	29.4	54.3
Ba	14.6	29.6	25.4	25.3	29.3	34.8	25.1	31.6	31.8	37.1	20.2	27.4	15.0	8.8	81.9	55.7	31.5	88.6
La	14.1	34.9	36.4	49.2	49.4	47.2	44.8	51.0	57.2	61.2	11.7	18.8	13.2	12.5	53.2	38.9	21.7	50.9
Ce	42.9	98.2	98.4	128	128	126	122	134	148	154	33.5	52.5	37.5	35.3	136.1	100.4	62.3	129.9
Pr	7.10	11.22	11.02	14.09	14.06	14.01	13.61	14.84	16.11	16.38	5.58	7.87	5.78	5.64	14.90	11.04	8.26	14.39
Nd	32.0	41.8	40.5	51.5	51.8	51.4	50.8	54.1	58.3	58.9	26.5	33.2	25.1	25.6	54.3	40.5	27.5	53.7
Sm	14.2	10.8	9.7	11.7	11.8	12.3	12.6	12.4	12.6	12.1	12.1	12.1	9.9	11.2	13.0	10.7	9.5	13.0
Eu	0.02	0.10	0.14	0.17	0.20	0.18	0.16	0.18	0.24	0.28	0.08	0.08	0.07	0.07	0.18	0.17	0.01	0.26
Gd	14.4	10.1	9.0	10.5	10.7	11.4	12.0	11.3	11.2	10.4	14.3	13.0	11.0	13.8	12.6	11.1	7.6	12.1
Tb	3.55	2.05	1.78	2.02	2.08	2.29	2.38	2.18	2.02	1.94	3.19	2.97	2.61	3.38	2.59	2.42	1.89	2.33
Dy	25.0	13.4	11.5	13.0	13.4	15.0	15.7	14.0	12.4	12.6	21.0	20.5	18.8	24.8	17.7	16.7	12.7	14.4
Ho	5.37	2.91	2.48	2.80	2.88	3.24	3.40	3.00	2.61	2.72	4.31	4.60	4.25	5.68	3.99	3.70	2.51	3.00
Er	16.40	8.69	7.39	8.35	8.59	9.61	10.05	8.89	7.56	8.32	11.79	13.70	13.04	17.75	11.95	10.97	7.87	8.69
Tm	2.78	1.40	1.17	1.30	1.35	1.49	1.56	1.38	1.16	1.32	1.75	2.16	2.11	2.88	1.81	1.71	1.49	1.32
Yb	19.76	9.61	8.12	8.85	9.16	10.04	10.64	9.35	7.60	9.00	11.35	14.77	14.72	20.06	11.83	11.48	11.52	8.92
Lu	2.95	1.46	1.22	1.32	1.39	1.50	1.59	1.41	1.13	1.36	1.65	2.24	2.26	3.09	1.73	1.69	1.72	1.36
Hf	8.31	6.88	5.52	5.98	7.31	6.03	6.99	6.84	7.46	7.68	6.03	7.93	6.77	7.78	6.50	4.36	5.48	6.83
Ta	16.61	9.29	12.20	8.12	8.44	7.84	9.23	7.58	6.71	7.13	11.58	12.64	13.12	16.36	6.39	7.69	45.81	8.74
Pb	52.4	55.8	60.2	210	59.7	55.6	51.8	46.9	52.8	61.4	57.9	64.0	175	16.1	47.5	60.41	69.26	49.66
Th	25.0	43.0	82.1	84.5	89.1	87.1	88.2	90.3	101	88.1	31.3	46.0	34.5	43.7	52.44	36.65	18.33	53.53
U	23.8	29.9	31.0	28.9	30.6	32.2	32.4	30.8	31.5	28.2	32.7	39.8	33.9	44.7	34.51	33.31	20.91	30.96
ΣREE	200	247	239	303	305	306	301	318	338	351	159	199	160	182	336	262	177	314

fine powders of 200 – mesh after drying and handpicking to remove visible alteration. Major element oxides were analyzed using the standard X-ray fluorescence (XRF) method given by Li et al. (2006b). Trace elements were determined using the inductively coupled plasma mass spectrometry (ICP-MS) method on a Perkin-Elmer Sciex ELAN 6000 instrument at the SKLIG GIG-CAS. The analytical procedures are the same as those described by Li et al. (2006b). Analytical precision for most trace elements is better than 3%. Geochemical results are listed in Tables 4 and 5.

4.4. Sr–Nd isotope analyses

Whole rock Rb–Sr and Sm–Nd isotope compositions were determined for 13 representative granite samples. Sr and Nd isotopic compositions were analyzed on a Micromass Isoprobe multi-collector ICP-MS at SKLIG GIG-CAS, and the analytical procedures follow those Li et al. (2006b). Sr and REE were separated using cation columns, and Nd fractions were further separated by passing through cation columns followed by HDEHP-coated Kef columns. Measured $^{87}\text{Sr}/^{86}\text{Sr}$ and $^{143}\text{Nd}/^{144}\text{Nd}$ ratios were normalized to $^{86}\text{Sr}/^{88}\text{Sr} = 0.1194$ and $^{146}\text{Nd}/^{144}\text{Nd} = 0.7219$, respectively. The reported $^{87}\text{Sr}/^{86}\text{Sr}$ and $^{143}\text{Nd}/^{144}\text{Nd}$ ratios were adjusted to the NBS SRM 987 standard $^{87}\text{Sr}/^{86}\text{Sr} = 0.710250$ and the Shin Etsu JNDI-1 standard $^{143}\text{Nd}/^{144}\text{Nd} = 0.512115$, respectively. The results, along with the calculated initial $^{87}\text{Sr}/^{86}\text{Sr}$ (I_{Sr}) and $\varepsilon_{\text{Nd}}(T)$ values, are listed in Table 6.

5. Results

5.1. Zircon U–Pb geochronology

Most of the zircon grains from two samples (ZK10C02-13 and ZK14B04-02) are euhedral and prismatic with aspect ratios of 1:1–3:1 and lengths of 100–300 μm . They are transparent and light yellow in color under the optical microscope. Ubiquitous simple internal oscillatory zoning and little inherited cores are displayed in CL images (Fig. 5b and d), which is typical for magmatic zircon in A-type granite (e.g. Wong et al., 2009). LA-ICP-MS zircon U–Pb isotopic data for these rocks are presented in Table 2. Zircon U–Pb concordia diagrams are shown in Fig. 5.

Twenty-three spot analyses of zircons from sample ZK10C02-13 yielded a single $^{206}\text{Pb}/^{238}\text{U}$ age population of 149.4–154.7 Ma with a weighted mean of 151.7 ± 1.2 Ma (MSWD = 0.30) (Table 2 and Fig. 5a), which represents the crystallization age of the granite. These zircons have highly variable abundance of Th (192–1257 ppm) and U (354–7047 ppm) contents, but their Th/U ratios change within a narrow range of 0.41–0.60 (except for the ratios of three sample varying from 0.18 to 0.36). Seventeen spot analyses of zircons from sample ZK14B04-02 yielded a single $^{206}\text{Pb}/^{238}\text{U}$ age population of 148.9–155.5 Ma with a weighted mean of

151.8 ± 1.4 Ma (MSWD = 0.63) (Table 2 and Fig. 5c), representing the formation age of the granites. These zircons have Th and U contents of 91–480 ppm and 162–1273 ppm, respectively, and their Th/U ratios range from 0.27 to 0.80. All the analyses are plotted on the concordia curve as a coherent group. Our zircon U–Pb dating results indicate that the Xitian granite was formed at ca. 152 Ma.

5.2. Hf isotopic composition

The analytical results on Hf isotopes for zircons from sample ZK14B04-02 are shown in Table 3. The initial $^{176}\text{Hf}/^{177}\text{Hf}$ ratios range from 0.282263 to 0.282469 with an average value of 0.282420. They have $\varepsilon_{\text{Hf}}(t)$ values of -14.69 to -7.43 (Fig. 6) with two stage model ages varying from 1338 to 1695 Ma.

5.3. Major and trace-element geochemistry

The results on major and trace-element compositions for a total of 43 Xitian granite samples are given in Tables 4 and 5. The Xitian granite is characterized by high SiO_2 (73.44–78.45 wt.%), moderate Al_2O_3 (11.20–13.90 wt.%) and highly variable Na_2O (0.01–4.24 wt.%) contents. Some samples have low Na_2O that may be due to hydrothermal alteration or the intense interactions between melts and fluids (Andersen et al., 1990). In the A/CNK (molar $\text{Al}_2\text{O}_3/(\text{CaO} + \text{Na}_2\text{O} + \text{K}_2\text{O})$) versus A/NK (molar $\text{Al}_2\text{O}_3/(\text{Na}_2\text{O} + \text{K}_2\text{O})$) diagram (Fig. 7), most of the samples plot in the area of metaluminous to weak peraluminous, except some samples which show strong peraluminous as a consequence of low Na_2O contents. These granites have moderate K_2O (2.87–5.87 wt.%), with all the samples plotting in the calc-alkaline and alkaline fields of K_2O versus SiO_2 diagram (Peccerillo and Taylor, 1976) (Fig. 7). Additionally, they also have low Fe_2O_3 (0.69–2.07 wt.%), MgO (0.003–0.42 wt.%), CaO (0.25–2.22 wt.%), TiO_2 (0.03–0.19 wt.%) and P_2O_5 (0.004–0.04 wt.%) contents. Major element variations are also shown in Harker diagrams, in which most of the samples give a similar variation trend without a compositional gap (Fig. 8).

The Xitian granites exhibit enriched REEs (except Eu) with total REE ranging from 159 to 351 ppm. Most of the granite samples are characterized by slightly enriched light REE (LREE) ($(\text{La}/\text{Yb})_N = 1.35$ –5.40) and flat heavy REE (HREE) with strong negative Eu anomalies ($\delta\text{Eu} = 0.004$ –0.08) (Fig. 9). All of the samples have low Sr (6.71–26.94 ppm), high Nb (23.70–52.47 ppm) and extremely high Rb (662–1119 ppm) contents, and are enrichment in high-field strength elements (HFSEs) (e.g. Nb, Ta, Zr and Hf).

5.4. Sr–Nd isotope compositions

The results on Sr–Nd isotopic analyses for the Xitian granite are given in Table 6. Initial Sr–Nd isotopic compositions were

Table 6
Sr–Nd isotopic compositions of the of Xitian granite.

Sample	Rb (ppm)	Sr (ppm)	$^{87}\text{Rb}/^{86}\text{Sr}$	$^{87}\text{Sr}/^{86}\text{Sr} \pm 2\sigma$	$(^{87}\text{Sr}/^{86}\text{Sr})_i$	Sm (ppm)	Nd (ppm)	$^{147}\text{Sm}/^{144}\text{Nd}$	$^{143}\text{Nd}/^{144}\text{Nd} \pm 2\sigma$	$\varepsilon_{\text{Nd}}(t)$	T_{DM2} (Ga)
ZK10C02-01	572	26.9	62.05753	0.817083 ± 13	0.68326	14.2	32.0	0.2685	0.512255 ± 9	-8.87	1.69
ZK10C02-07	940	10.8	262.28846	1.156539 ± 16	0.59092	9.7	40.5	0.1454	0.512213 ± 9	-7.30	1.56
ZK10C02-12	904	14.6	185.75187	1.063792 ± 17	0.66323	11.7	51.5	0.1374	0.512180 ± 8	-7.79	1.60
ZK10C02-17	852	11.2	228.02762	1.107928 ± 18	0.61620	12.3	51.4	0.1450	0.512137 ± 9	-8.78	1.68
ZK10C02-20	801	15.1	158.07017	0.981477 ± 14	0.64060	12.4	54.1	0.1383	0.512136 ± 8	-8.67	1.68
ZK10C02-25	662	14.7	133.38406	0.928352 ± 13	0.64071	12.1	58.9	0.1240	0.512117 ± 10	-8.76	1.68
ZK10C02-30	1119	20.7	160.31538	0.983268 ± 17	0.63755	12.1	33.2	0.2204	0.512213 ± 10	-8.76	1.68
ZK10C02-33	946	6.7	436.55843	1.433913 ± 30	0.49249	9.9	25.1	0.2379	0.512221 ± 8	-8.93	1.70
ZK10C02-36	825	7.0	359.56898	1.307626 ± 19	0.53223	11.2	25.6	0.2649	0.512265 ± 9	-8.60	1.67
ZK14B04-02	882	16.3	161.16039	0.988169 ± 15	0.64040	13.0	54.3	0.1442	0.512113 ± 8	-9.23	1.72
ZK14B04-07	790	14.1	166.77728	0.999358 ± 15	0.63947	10.7	40.5	0.1596	0.512142 ± 10	-8.96	1.70
ZK14B04-12	682	13.5	150.29545	0.973005 ± 18	0.64868	9.5	27.5	0.2091	0.512178 ± 9	-9.22	1.72
ZK14B02-01	727	21.4	100.03186	0.889120 ± 13	0.67326	13.0	53.7	0.1460	0.512121 ± 8	-9.11	1.71

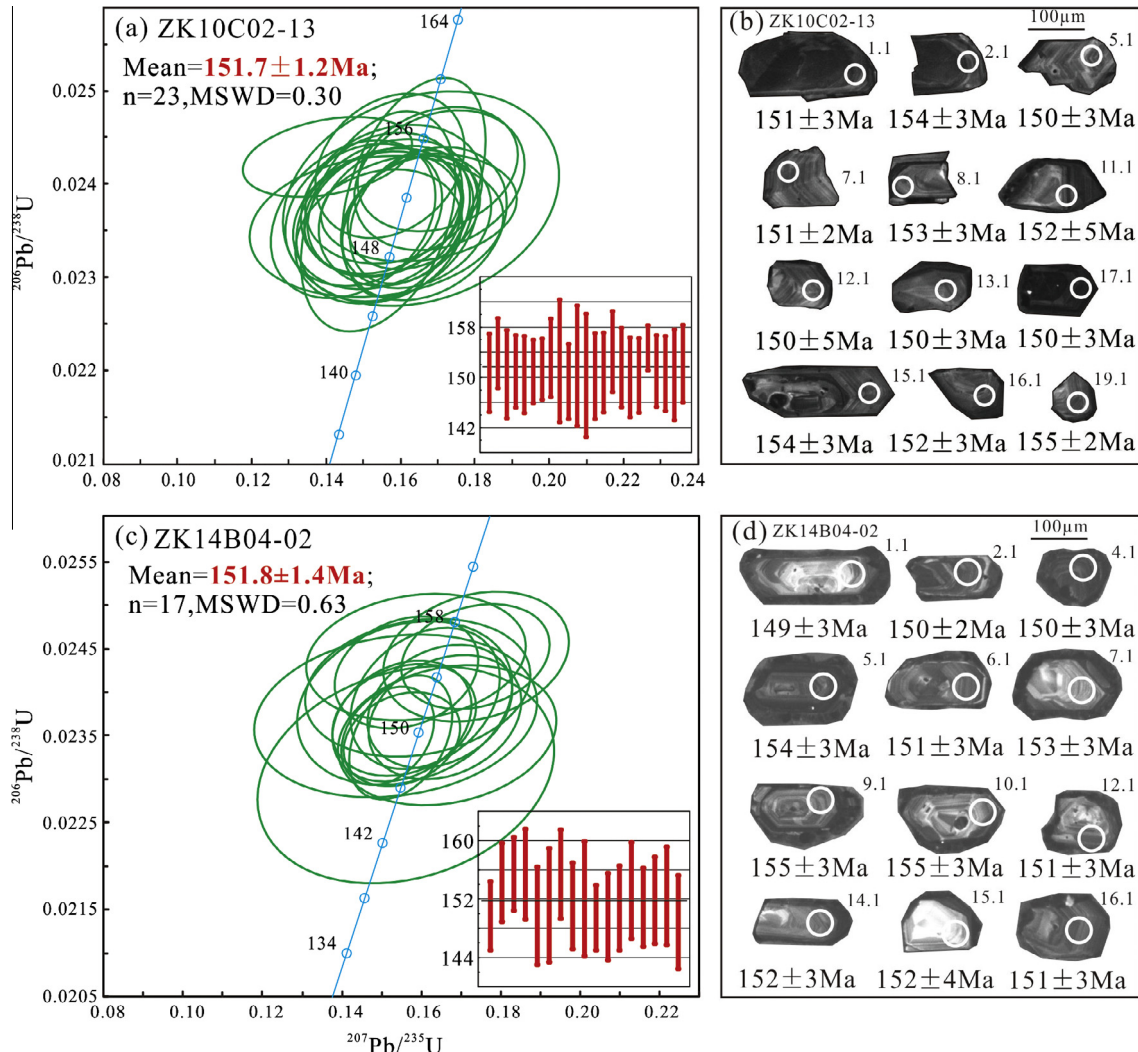


Fig. 5. Zircon U-Pb concordia diagrams and representative cathodoluminescence (CL) images for the Xitian granite.

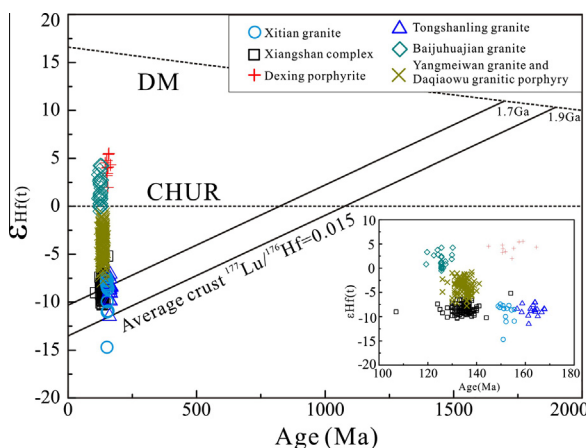


Fig. 6. Evolution of $\epsilon_{\text{Hf}}(t)$ versus age (Ma) of the Xitian granite. Data of the Xiangshan volcanic-intrusive complex, Dexing porphyrite, Tongshanling granite, Baijuhuajian granite, Yangmeiwan granite and Daqiaowu granitic porphyry are from Yang et al. (2011), Zhou et al. (2012a), Jiang et al. (2009), Wong et al. (2009) and Yang et al. (2012), respectively. DM: depleted mantle; CHUR: Bulk Earth (chondritic uniform reservoir).

calculated at $t = 152$ Ma. They have $\epsilon_{\text{Nd}}(t)$ values ranging from -9.23 to -7.30 and $(^{143}\text{Nd}/^{144}\text{Nd})_i$ from 0.511926 to 0.512069 .

The corresponding two-stage depleted mantle Nd model ages ($T_{\text{DM}2}$) are in the range of 1562 – 1722 Ma.

6. Discussion

6.1. Origin of granitic rocks: an A-type affinity

As currently known only on Earth, granitic rock plays an extremely important role in the evolution of the Earth's crust and its formation and evolution must be accompanied by migration and/or enrichment of elements, which is likely to form important ore deposits. Traditionally, granitic rocks can be divided into S-, I- and M- types granites based on their different sources (Chappell and White, 2001; Collins et al., 1982; Whalen et al., 1987). The term of "A-type granite" was first proposed by Loiselle and Wones (1979) to define a series of granitic rocks that distribute in extensional tectonic environments such as anorogenic backgrounds or rift zones. Subsequently, Eby (1992) divided A-type granites into two subclasses: A₁ and A₂ types. A-type granites have some common geochemical characters such as high TiO_2/MgO , $\text{K}_2\text{O}/\text{Na}_2\text{O}$, and Fe/Mg ratios. They also possess high K_2O and SiO_2 contents and low CaO , Ba and Sr contents and enriched F , Nb , Ta , Zr , Ga , Y and REEs (except Eu) (Douce, 1997; Loiselle and Wones, 1979; Whalen et al., 1987), but low levels of elements compatible in mafic silicates (Cr, Ni, Co

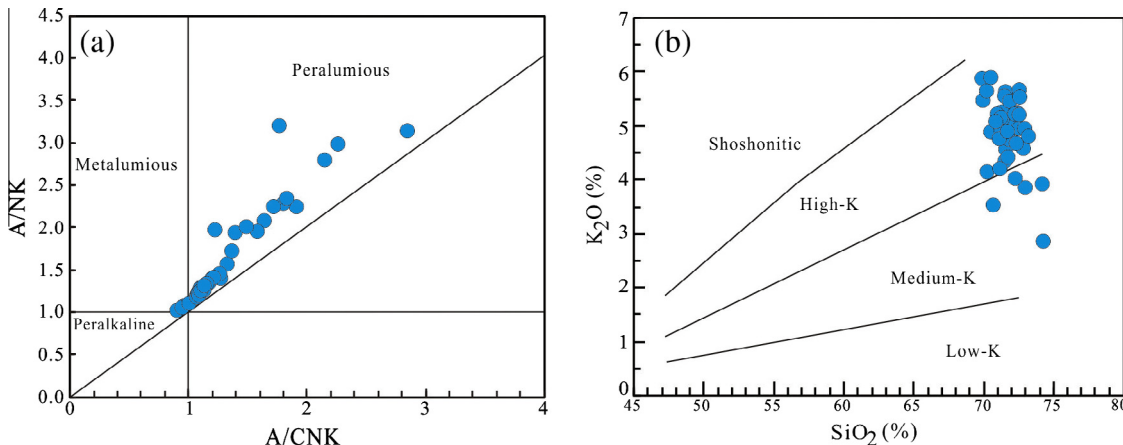


Fig. 7. Plot of (a) A/NK versus A/CNK and (b) K_2O versus SiO_2 . $A/NK = Al_2O_3/(Na_2O + K_2O)$ (molar ratio), $A/CNK = Al_2O_3/(CaO + Na_2O + K_2O)$ (molar ratio).

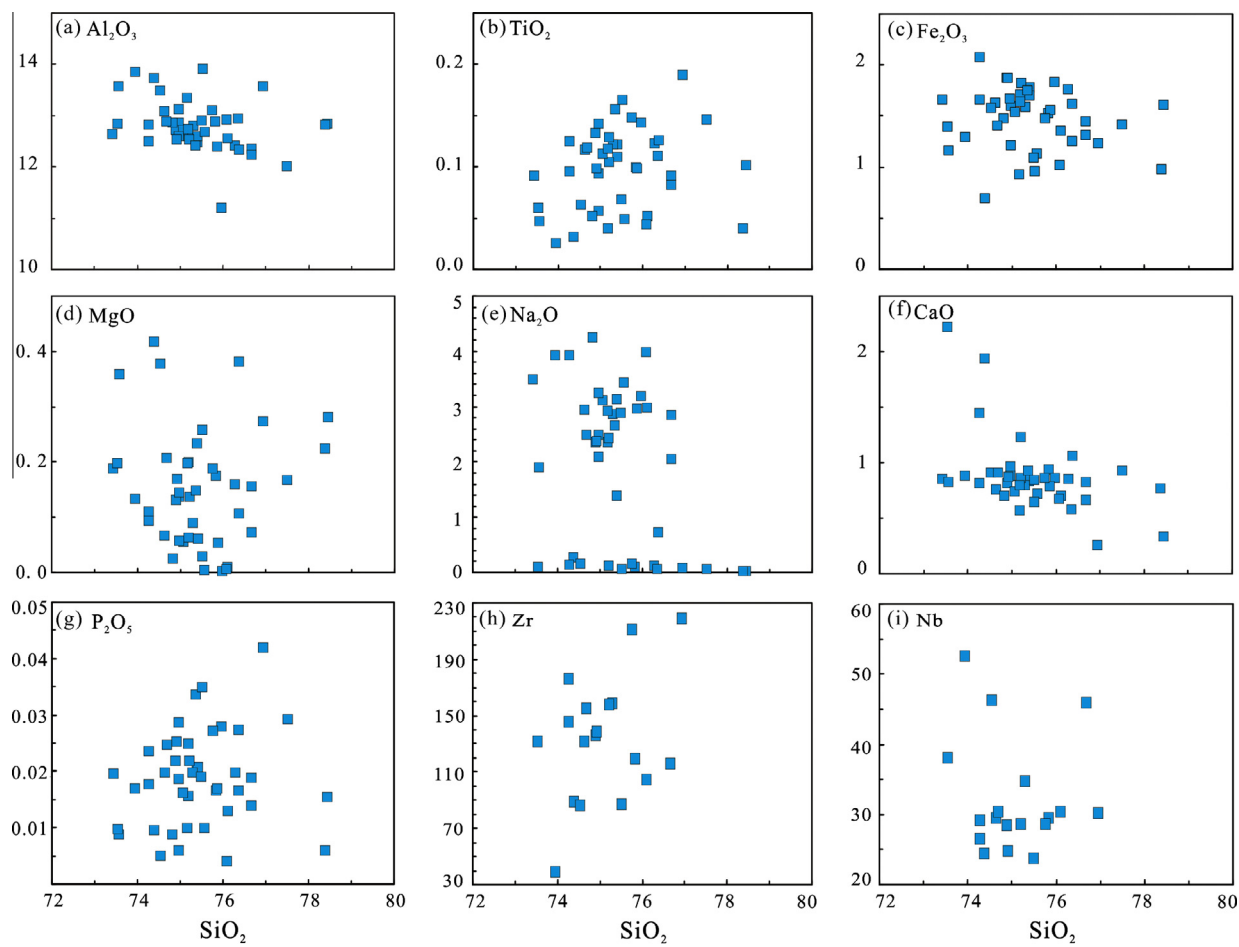


Fig. 8. Harker diagrams for the Xitian granite samples.

and Sc) and feldspars (Sr, Ba and Eu) (Loiselle and Wones, 1979). Petrographically, A-type granites generally involve Fe-rich biotite or/and alkali hornblendes and are lack of inherited zircon grains (Williams, 1992), whereas S-type granites contain abundance of Al-rich minerals such as muscovite, garnet, and cordierite. The feldspar in A-type granites is mostly alkali feldspar, into which micrographic intergrowths of quartz are usually observed. Mafic minerals commonly crystallize late in the solidification history, representatively existing as interstitial clots or grains (Whalen

et al., 1987). Besides, A-type granites usually exhibit mineralization by Sn, W, Mo, Bi, Nb and F (Collins et al., 1982).

The Xitian granites in this study have moderate to high total alkalis ($K_2O + Na_2O = 2.89\text{--}8.98$ wt.%) and low Al_2O_3 (<13.90 wt.%) contents. With respect to I-type granites, most of the Xitian granites have higher A/CNK (0.90–1.27) and Fe^* values [$FeOt/(FeOt + MgO) = 0.60\text{--}1.00$]. Compared with S-type granites, they are characterized by extremely low P_2O_5 (0.004–0.04 wt.%) abundances and absence of phosphate minerals. Additionally, they have

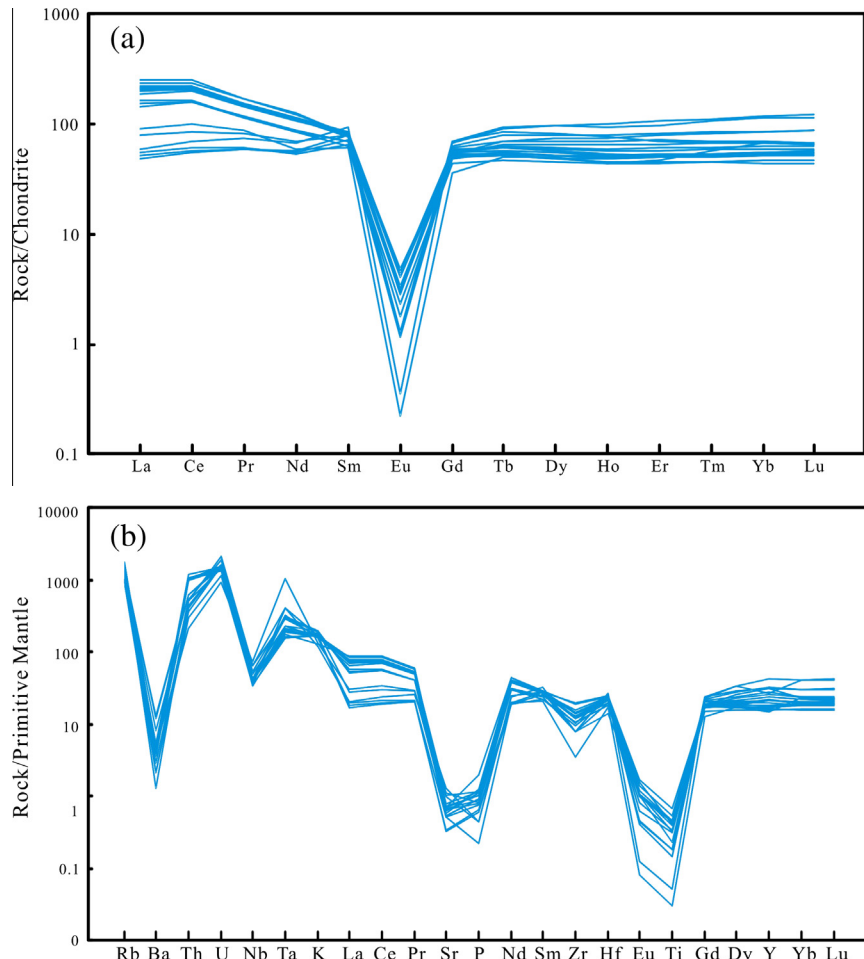


Fig. 9. Chondrite-normalized REE patterns and primitive mantle-normalized incompatible trace element spidergrams for the Xitian granite. The normalized values for the chondrite and primitive mantle are from Sun and McDonough (1989).

enriched HFSE (e.g., Nb) and REE, and obviously depleted Si, Ba, P, Ti and Eu, similar to the trace-element compositions of A-type granites (Li et al., 2007c; Fig. 9). Most of the Xitian granites have significantly lower Sr contents (<30 ppm) than typical calc-alkaline I-type granites. According to Douce (1997), Sr contents is an important sign to discriminate A-type granites from calc-alkaline granites because the Sr contents in the former are only around 33–50% of those in the latter at the same SiO₂ level. Therefore, the extraordinary low Sr contents is also likely indicative of the Xitian granites as A-type. Their low La/Nb (0.25–2.15), Nb/Ta (1.15–4.25) and Zr/Hf (7.00–28.46) ratios are consistent with those in typical A-type granites (e.g. Eby, 1992; King et al., 1997; Martin et al., 1994). Moreover, the Xitian granites show Fe-rich biotite and enrichment in alkalis (Table 1 and Fig. 3b, d, Fig. 4). All lithological and geochemical characters of the Xitian granite indicate that they have an affinity of A-type rather than S- and I-types granite (Bonin, 2007; King et al., 1997). Their high Ce/Nb and Y/Nb ratios (Fig. 10c) further suggest that they belong to the A₂-type granites (Eby, 1992). Most of the samples fall into the area of “within-plate granite” in the diagrams of Pearce et al. (1984) (Figures not shown) and plot in the field of “A-type granites” in the discrimination diagrams of Whalen et al. (1987) and Eby and Kochhar (1990) (Fig. 10), further verifying their A-type affinity.

Numerous A-type granites have been identified along the Shi-Hang zone in the past decade, such as the Jiuyishan (Huang et al., 2011), Qianlishan (Jiang et al., 2006), Xiangshan (Jiang et al., 2005), Qitianling (Li et al., 2010b), Damaoshan (Jiang et al.,

2011), Baijuhuajian (Wong et al., 2009), Tongshan (Jiang et al., 2011) and Yangmeiwan granites (Yang et al., 2012), Daqiaowu granitic porphyry (Yang et al., 2012), and Huashan-Guposhan intrusive belt (Zhu et al., 2006a), etc. These A-type granites, together with the Xitian A-type granite recognized in this study, indicate that the Shi-Hang Zone is an important magmatic zone composed mainly of A-type granites.

6.2. Petrogenesis of the Xitian granite

It is widely accepted that no general petrogenetic model can be responsible for all A-type granites due to their widespread distribution, the diversity of tectonic settings in which they formed, the complexity of associated rocks, and the large geochemical differences in major and trace element and Sr–Nd isotopic compositions between different A-type granitic intrusions (e.g. Anderson et al., 2003; Collins et al., 1982; Martin, 2006; Su et al., 2007; Whalen et al., 1987). To date, several mechanisms have been proposed for explaining the origin of A-type granitic magma: (1) efficient fractional crystallization of a mantle-derived mafic magma, with or without accompanying assimilation (Anderson et al., 2003; Han et al., 1997; Turner et al., 1992); (2) partial or complete melting of an alkali-metasomatized crust (Martin, 2006); (3) melting of deep crust materials such as granulitic residue from which hydrous felsic melts were previously extracted (Collins et al., 1982; Whalen et al., 1987); and (4) melting of tonalitic I-type granites (e.g., Skjerlie and Johnston, 1993). Of primary

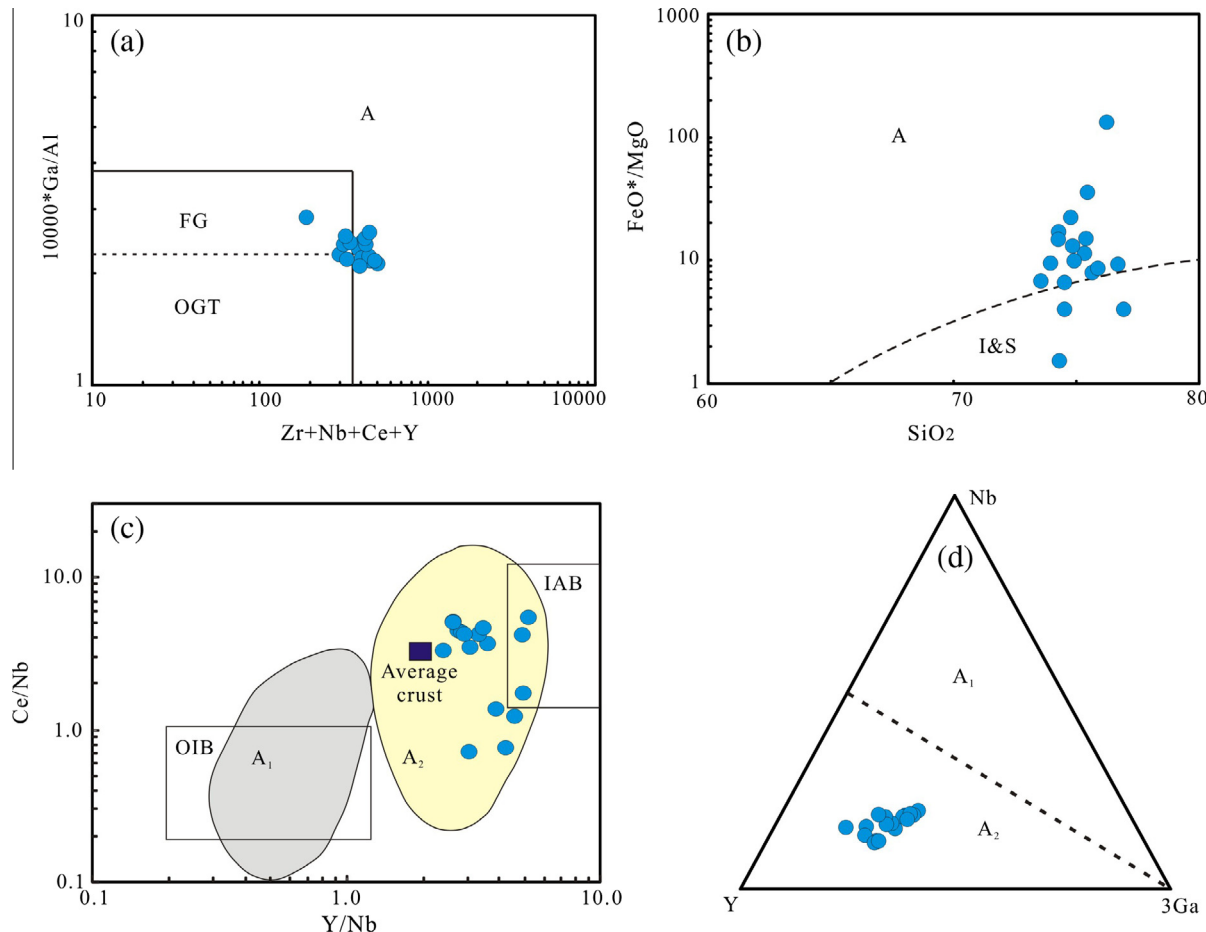


Fig. 10. (a) 10000 Ga/Al versus Zr + Nb + Ce + Y (Whalen et al., 1987), (b) FeO*/MgO versus SiO₂ (Eby and Kochhar, 1990), (c) Ce/Nb versus Y/Nb (Eby, 1992), and (d) Nb-Y-3Ga (Eby, 1992) discrimination diagrams for Xitian granite.

concern is whether mantle-derived materials could be involved in the formation of A-type granites.

As shown in the primitive mantle-normalized trace element spidergram, Xitian granites show negative Eu, Ba and Sr anomalies (Fig. 9b), together with decreases in Sr and Ba with increasing SiO₂ (Figures not shown), indicative of plagioclase fractionation during the evolution of the Xitian granites. They also have pronounced negative anomalies in P and Ti (Fig. 9b), which could be attributed to the fractionation of apatite and ilmenite. There are moderate correlations between some of the major oxides (e.g., Al₂O₃ and CaO) and SiO₂ (Fig. 8), also support that magmas are fractionated to some degree during their evolution. They show high HFSEs and REEs (except Eu) concentration, suggestive of dark-colored minerals such as hornblende and biotite involved in their source. Intense fractional crystallization of granitic melt (including REE accessories) and its interaction with volatile-rich (e.g., F and Cl) fluid may be the main factors resulting in the tetrad effects of REE (Monecke et al., 2002; Zhao et al., 2002). Non-CHARAC (CHARGE-And-RADIUS-Controlled) trace element features such as high K/Ba, low Zr/Hf and K/Rb also indicate increasingly intense melt-rocks/fluids interactions (Bau, 1996; Chen et al., 2014; Jahn et al., 2001).

Nd isotopes are scarcely remobilised by hydrothermal alteration, thus they can be used as a powerful tool for revealing the genesis of A-type granites (Poitrasson et al., 1995). The Xitian A-type granites in this study have moderate to high negative $\varepsilon_{\text{Nd}}(t)$ values (-9.23 to -7.30), distinguishable from those of coeval mafic rocks (Fig. 11), indicating that they were unlikely formed by

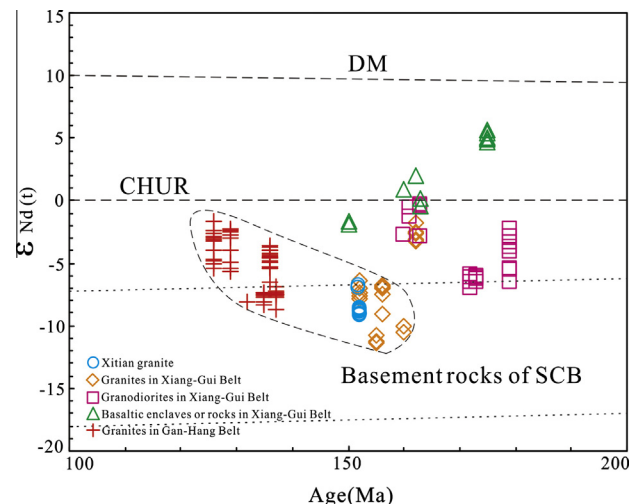


Fig. 11. Evolution of $\varepsilon_{\text{Nd}}(t)$ versus age (Ma) of igneous rocks from Shi-Hang Zone. The cited $\varepsilon_{\text{Nd}}(t)$ and age data are from Table 7. Data of basement rocks of South China Block are from Wang et al. (2013), Chen and Jahn (1998) and references therein. DM: depleted mantle. CHUR: Bulk Earth (chondritic uniform reservoir).

fractional crystallization from coeval mantle-derived mafic magmas. Instead, their Nd isotopic compositions show a close relationship to the granitoids from Precambrian basement rocks of the SCB (e.g. Chen and Jahn, 1998; Zhang et al., 2006; Zheng et al., 2006) (Fig. 11). These characters suggest that they mainly sourced from

remelting of ancient granitoids. This conclusion is further supported by their low $\varepsilon_{\text{Hf}}(t)$ values (-14.69 to -7.43) (Fig. 6) and high K₂O contents. Together with the extensively exist of mafic enclaves in the Xitian granites which were considered to be the product of mantle–crust interaction (Liu et al., 2008), this suggests that mantle-derived components were inputted into their sources. Like the Xitian granites, lots of other A-type granites (e.g., the Baijuhuajian, Damaoshan, Tongshan, Yangmeiwan and Daqiaowu granites) along the Shi-Hang zone also contain mafic enclaves that were supposed to represent the process of mantle–crust interaction (Jiang et al., 2005; Zhao et al., 2010; Zhu et al., 2006b), indicating that they may have a similar petrogenesis. The gradual increase $\varepsilon_{\text{Hf}}(t)$ and $\varepsilon_{\text{Nd}}(t)$ values indicate that more mantle components were involved in the sources from the early to late stages of magmatism (Figs. 6 and 11).

6.3. Tectonic significance

A-type granites are generally considered to form in extensional or post-orogenic tectonic environments, such as back-arc extension, post-collisional extension or within-plate settings, regardless of the origin of the magma source (e.g. Eby, 1992; Turner et al., 1992; Whalen et al., 1987). In terms of tectonic setting, Eby (1992) divided the A-type granites into two groups: (1) the A₁-type granites formed in anorogenic settings (e.g., hotspots, plumes or continental rift zones), and (2) the A₂-type granitoids emplaced in a variety of tectonic settings and their magmas are generated from crust that have been through a cycle of subduction-zone or continent–continent collision magmatism. As for the Xitian granites, we propose they could be formed in a back-arc extensional tectonic environment based on the following regional geological data: (1) The Shi-Hang zone exhibits NNE-trending, which is well consistent with the suture zone of subduction of the Paleo-Pacific plate beneath the SCB, but obviously different from the WE-trending Indosinian collision zone; (2) The Xiangshan volcanic complex from the Shi-Hang zone has also an A-type affinity and its quenched mafic enclaves are high-Mg potassic rocks with boninitic affinity (Jiang et al., 2005), indicating a back-arc extensional environment; (3) Contemporaneous bimodal magmatism occurred

in the Shi-Hang zone such as the Qianlishan, Jinjiling, Xishan and Tongshanling, implying a continental arc to intra-arc rifting setting due to slab rollback (Jiang et al., 2009 and references therein); and (4) Evidences such as radiating dike swarm, voluminous basalts and crustal doming for a Mesozoic mantle plume are lacking so far (Gilder et al., 1991; Li et al., 2007a), combine with the Xitian granites have an affinity of A₂-type granites (Fig. 10c–d), ruling out an origin related to hotspot, plume or continental rift zone located in anorogenic settings. Consequently, it is herein proposed that the formation of the ~152 Ma Xitian granites were related to back-arc extension which was caused by the subduction of Paleo-Pacific plate beneath the Eurasian plate.

According to Li et al. (2010a), four distinct episodes of A-type granitic rocks, 195–170 Ma, 170–150 Ma, 137–122 Ma and 110–90 Ma, and two “magmatic quiescence” of ca. 150–140 Ma and ca. 120–110 Ma were distinguished in SE China. A prevalent point of view is that the formation of the Late Mesozoic igneous rocks in SE China was related to subduction of the Paleo-Pacific plate and underplating of mafic magmas (Faure and Natalin, 1992; Martin et al., 1994; Yang et al., 2012; Zhou and Li, 2000; Zhou et al., 2013; Li et al., 2012; Meng et al., 2012; Huang et al., 2013; Zhu et al., 2014). In the Early–Middle Jurassic (180–160 Ma), the Paleo-Pacific plate was subducted beneath the SCB with a very low angle (Tatsumi and Eggins, 1995) along the eastern flank of the Central Range in Taiwan. Due to temperature and pressure increases, sediments and hydrous minerals (e.g., talc, chlorite, and serpentine, etc.) on the subducting Paleo-Pacific plate dehydrated to release fluids, which fluxed the overlying mantle wedge to produce basaltic magmas. Such magmas then underplated and heated the lower continental crust where they finally triggered intracrustal melting to generate the 180–160 Ma plutons in SE China. Around or above the melt zone, a large amount of the source region dehydrated to provide source materials for A-type magmas and ultimately formed a series of ca. 160 Ma A-type granites along the Shi-Hang Zone (e.g. Jiang et al., 2005).

The dip angle of the subducted Paleo-Pacific plate increased during 160–135 Ma (Maruyama and Seno, 1986; Xia and Zhao, 2014), giving rise to oceanward migration of the active magmatic zone, and this is the most likely reason why the A-type plutons

Table 7
Synthesis of the ages and Sr–Nd isotopic compositions of the igneous rocks along Shi-Hang zone.

Pluton	(⁸⁷ Sr/ ⁸⁶ Sr)i	$\varepsilon_{\text{Nd}}(t)$	Age (Ma)	Method	Reference
Xihunshan granite	0.7163–0.7169	-10.7 to -11.4	150–153	SHRIMP zircon c	Lv et al. (2011), Shen et al. (1994)
Jiufeng granite	0.7161–0.7165	-10.0 to -10.5	154 ± 1	Single-grain zircon U–Pb	Li (1991), Yin et al. (2010)
Xitian granite	0.5909–0.6832	-8.9 to -7.3	151 ± 2	LA-ICPMS zircon U–Pb	This study
Qianlishan granite	0.7072–0.7182	-5.0 to -11.5	152 ± 2	SHRIMP zircon U–Pb	Li et al. (2004b)
Qitianling granite	0.7083–0.7108	-6.8 to -5.0	155 ± 1	SHRIMP zircon U–Pb	Zhao et al. (2006)
Xishan granite	0.7161–0.7182	-7.0 to -9.1	156 ± 2	SHRIMP zircon U–Pb	Fu et al. (2004)
Jinjiling granite	0.7142–0.7272	-6.3 to -7.1	156 ± 2	SHRIMP zircon U–Pb	Fu et al. (2004), Jiang et al. (2009)
Huashan granite	0.7063–0.7071	-3.2 to -2.7	162 ± 1	SHRIMP zircon U–Pb	Zhu et al. (2006a,b)
Guposhan granite	0.7066–0.7074	-3.1 to -1.7	162 ± 3	SHRIMP zircon U–Pb	Zhu et al. (2006a,b)
Tongshanling granodiorite	0.7085–0.7104	-6.6 to -2.3	164 ± 2	SHRIMP zircon U–Pb	Wang et al. (2003), Jiang et al. (2009)
Baoshan granodiorite	0.7095–0.7103	-5.9 to -7.0	158 ± 2	SHRIMP zircon U–Pb	Wang et al. (2003), Li et al. (2006)
Shuikoushan granodiorite	0.7088–0.7102	-6.0 to -6.5	163 ± 2	SHRIMP zircon U–Pb	Wang et al. (2003), Ma et al. (2006)
Niumao granodiorite	0.7047–0.7051	-0.5 to -1.3	163 ± 4	SHRIMP zircon U–Pb	Zhu et al. (2005)
Tong'an monzonite	0.7051	-0.4	160 ± 4	SHRIMP zircon U–Pb	Zhu et al. (2005)
Mafic enclaves in Huashan-Guposhan granite	0.7047–0.7057	-0.5 to 1.9	162 ± 2	SHRIMP zircon U–Pb	Zhu et al. (2006a,b)
Ningyuan alkali basalt	0.7035–0.7040	+5 to +6	175	Total rock 40Ar/39Ar	Li et al. (2004a), Jiang et al. (2009)
Daixian high-Mg basalt	0.7054	-1.6 to -1.9	150	Total rock 40Ar/39Ar	Li et al. (2004a), Jiang et al. (2009)
Dexing granodiorite	0.7044–0.7047	-1.14 to +1.80	171–154	SHRIMP zircon U–Pb	Zhou et al. (2012a), Wang et al. (2004b)
Xiangshan	0.7085–0.7151	-6.86 to -8.73	137–135	SHRIMP/LA-ICPMS zircon U–Pb	Yang et al. (2011)
Daqiaowu	0.7088–0.7097	-4.41 to -6.47	136–133	SHRIMP/LA-ICPMS zircon U–Pb	Yang et al. (2012)
Yangmeiwan	0.7073	-3.57 to -4.51	136 ± 2	SHRIMP zircon U–Pb	Yang et al. (2012)
Tongshan	0.7080–0.7089	-2.2 to -5.6	129 ± 2	SHRIMP zircon U–Pb	Jiang et al. (2011)
Baijuhuajian	0.7917	-2.6	126 ± 3	SHRIMP zircon U–Pb	Wong et al. (2009)
Damaoshan	0.70803	-1.7 to -5.4	126–122	SHRIMP zircon U–Pb	Jiang et al. (2011)

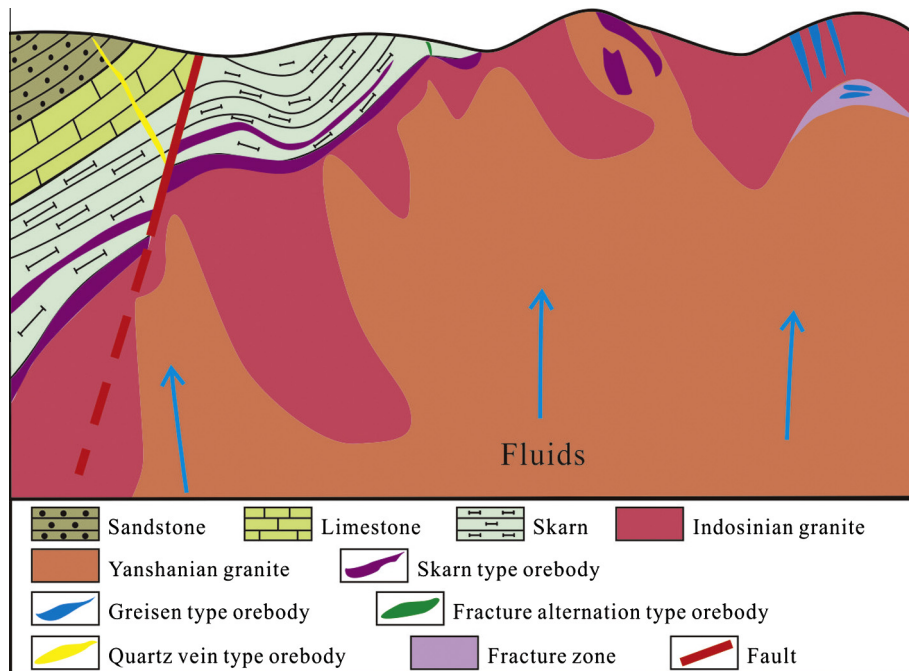


Fig. 12. Metallogenetic model of the Xitian W-Sn polymetallic deposit (modified from Wu et al., 2012). Indosinian granite emplaced into Devonian carbonatite, forming fracture zones and massive skarn which was further superimposed by mineralization of the Yanshanian granite modified by the fluid released in the process of mantle–crust interaction. The superimposed processes finally formed the skarn, greisen, quartz vein and W-Sn polymetallic deposits of the fracture zone type.

commonly become younger toward the coast in SE China (e.g. Wong et al., 2009; Sun et al., 2015). Rollback of the Paleo-Pacific plate led to back-arc extension and finally formed the ca. 150 Ma A-type granites along the Shi-Hang Zone. With ongoing back-arc extension during slab rollback, the crust and lithospheric mantle became progressively thinned. Our element geochemical data, along with previous data, indicate that the mantle–crust interaction in the formation of the A-type granitic magma along the Shi-Hang zone were gradually intensified from the early to late phases of magmatism, resulting in higher $\varepsilon_{\text{Nd}}(t)$ values in the late stages of magmatism (Table 7 and Figs. 6 and 11). This also explains why a series of localized extensional red-bed basins developed throughout the Late Mesozoic (e.g. Gilder et al., 1996; Zhou et al., 2006). Therefore, it is most likely that the Shi-Hang zone is part of a back-arc extensional zone in SE China, which, together with its resulting upwelling of asthenosphere, led to partial melting of the phlogopite-bearing spinel harzburgitic lithospheric mantle, generating the high-Mg potassic rocks that resulted in mafic enclaves (Jiang et al., 2005). This is further supported by the Daoxian high-Mg basalts (Li et al., 2004a) and the existence of mafic enclaves hosted by most of the A-type granites along the Shi-Hang zone (Jiang et al., 2005; Zhao et al., 2010; Zhu et al., 2006b; this study).

6.4. The relationship between granitic magmatism and tungsten-tin mineralization

Previous studies suggested that tungsten-tin mineralization was mainly related to S-type granitoids (Heinrich, 1990; Tanelli, 1982). In recent years, a growing number of studies show that W-Sn mineralization is also closely associated with the A-type granitoids (e.g., Bastos Neto et al., 2009; Botelho and Moura, 1998; Haapala and Lukkari, 2005; Zhou et al., 2012b). Yanshanian is an important metallogenetic period in SE China, forming two styles of ore systems, i.e., W-Sn polymetallic deposits and skarn and porphyry copper deposits (Mao et al., 2009). The Xitian granites

located at the middle part of Shi-Hang Zone are composed of the Indosinian and Yanshanian granites. Most of the deposits veins are spread in the outer contact zone of the Indosinian granites (Fig. 12), but the following several geological characteristics indicate that the Yanshanian granites have a close relationship with the giant Xitian W-Sn polymetallic deposit.

- (1) Drilling data indicate that thick Yanshanian granite distributed under the Indosinian granite (Fu et al., 2012), and previous studies showed that the metallogenesis age of the Xitian tungsten-tin deposits was constrained at 157–150 Ma (Fu et al., 2012; Liu et al., 2008; Ma et al., 2008), close to the age of buried Early Yanshanian granite body determined in this study (ca. 152 Ma). This suggests that the tungsten-tin mineralization age is consistent with the granitic magmatism.
- (2) The Sn and W contents of the Early Yanshanian granite are 6–10 and 10–20 times of their Clark values, respectively, whereas the Indosinian granite has much lower Sn and W contents (Fu et al., 2012; Yao et al., 2013), indicating that the Early Yanshanian granite is closely tied to the W-Sn mineralization. They could provide ore-forming materials for the mineralization.
- (3) The Early Yanshanian granite is characterized by high Si (73.44–78.45 wt.%) and Rb (662–1119 ppm) contents, low Ti, P, Sr and Ba contents (Fig. 9 and Table 5), low Rb/Sr and Nb/Ta ratios (1.15–4.25) (Table 5), and REE patterns with pronounced tetrad effect (Fig. 9). These features suggest an intense fluid–magma interaction which is extremely favorable to W-Sn mineralization (Bastos Neto et al., 2009; Green, 1995; Jahn et al., 2001; Lehmann and Harmanto, 1990). In contrast to the Early Yanshanian granite, the Indosinian granite is an intermediate to acidic igneous rock and has higher Ti, P, Sr and Ba contents, but lower Si, Rb and Nb/Ta values and right-dipped REE patterns (Yao et al., 2013), different from those of W-Sn mineralized granite.

Previous studies on fluid inclusions in fluorite and quartz showed that the fluids were mainly from mantle fluid (Yang et al., 2007). Country-rocks of the Xitian granite mainly include Devonian argillaceous limestone and dolomitic limestone, which were controlled by NE or NNE compress-shear fractures and NNW tensional and torsional fractures. These conditions are convenient for formation of ore skarn and migration and storage of ore-forming materials. Therefore, we propose that fluids from country-rocks and/or ground water heated by granitic magma in the late stage play an important role in activating and enriching metallogenic materials during mineralization.

In conclusion, the intrusions of the Indosinian granite only resulted in preliminary enrichment of ore-forming materials, but low grade tin and tungsten do not achieve the industrial grade. The ore-forming materials and fluids were dominantly produced by the Early Yanshanian granitic magmatism to form the Xitian W-Sn orebody. Therefore, the Xitian tungsten-tin mineralization shows a close relationship to the Early Yanshanian granitic activity. Considering the discussion above and other geological, geophysical and drilling data, a metallogenic model of the Xitian W-Sn polymetallic orefield is proposed in Fig. 12. The emplacement of the Indosinian granite not only caused the development of a fracture zone, but also formed massive skarn which was subsequently superimposed by mineralization of the Yanshanian granite. The intrusion of the Yanshanian granite formed greisen, quartz vein and a fracture alternation type W-Sn polymetallic orebody.

7. Conclusions

Geochemical data indicate that the Xitian granite in the eastern Hunan Province is a metaluminous to weak peraluminous granite with typical geochemical signatures of A-type granites, such as high Fe^* values, K_2O/Na_2O ratios and extremely low P_2O_5 contents, enrichments in incompatible elements (HFSEs and REEs except Eu) but depletions in Ba, Sr and Eu. Involvement of Fe-rich biotite and alkali feldspar in the Xitian granite also suggests an A-type affinity.

Zircon U-Pb dating shows that the Early Yanshanian granite from Xitian area was formed at ca. 152 Ma. Geochemical and isotopic data imply that they were generated by partial melting of metamorphic basement rocks with input of variable proportion of mantle-derived materials. They were most likely formed in a back-arc extensional tectonic environment caused by the subduction of the Paleo-Pacific plate. The mantle-crust interaction in the formation of the A-type granite along the Shi-Hang Zone were gradually intensified from the early to late stages of magmatism. The Early Yanshanian granite from Xitian has a close relationship to the W-Sn mineralization and provides ore-forming materials and fluids for the giant Xitian W-Sn deposit.

Acknowledgements

We would like to thank Haofeng Zhu and other colleagues from 416 Brigade, Bureau of Geology and Mineral Exploration and Development of Hunan Province for their help during fieldwork. Critical and constructive reviews by the reviewers and the associate editor Irene Yao are highly appreciated. This study was jointly supported by the Ministry of Natural Resources (201211024-03), the National Science and Technology Major Project of China (No. 2011ZX05023-004-11), Chinese Academy of Sciences (KZCX1-YW-15-1) and Natural Science Foundation of China (40872080 and 41072081).

References

- Andersen, T., 2002. Correction of common lead in U-Pb analyses that do not report Pb-204. *Chem. Geol.* 192 (1–2), 59–79.
- Andersen, T., Rankin, A.H., Hansteen, T.H., 1990. Melt-mineral-fluid interaction in peralkaline silicic intrusions in the Oslo Rift, SE Norway. III: alkali geothermometry based on bulk fluid inclusion content. *NGU Bull.* 417, 33–40.
- Anderson, I.C., Frost, C.D., Frost, B.R., 2003. Petrogenesis of the Red Mountain pluton, Laramie anorthosite complex, Wyoming: implications for the origin of A-type granite. *Precambr. Res.* 124 (2–4), 243–267.
- Bastos Neto, A.C., Pereira, V.P., Ronchi, L.H., DeLima, E.F., Frantz, J.C., 2009. The world-class Sn, Nb, Ta, F (Y, REE, Li) deposit and the massive cryolite associated with the albite-enriched facies of the Madeira A-type granite, Pitinga mining district, Amazonas state, Brazil. *Can. Mineral.* 47 (6), 1329–1357.
- Bau, M., 1996. Controls on the fractionation of isovalent trace elements in magmatic and aqueous systems: evidence from Y/Ho, Zr/Hf, and lanthanide tetrad effect. *Contrib. Miner. Petrol.* 123, 323–333.
- Black, L.P., Kamo, S.L., Allen, C.M., Aleinikoff, J.N., Davis, D.W., Korsch, R.J., Foudoulis, C., 2003. TEMORA 1: a new zircon standard for Phanerozoic U-Pb geochronology. *Chem. Geol.* 200 (1–2), 155–170.
- BlichertToft, J., Albarede, F., 1997. The Lu-Hf isotope geochemistry of chondrites and the evolution of the mantle–crust system. *Earth Planet. Sci. Lett.* 148, 243–258.
- Bonin, B., 2007. A-type granites and related rocks: evolution of a concept, problems and prospects. *Lithos* 97 (1–2), 1–29.
- Botelho, N.F., Moura, M.A., 1998. Granite-ore deposit relationships in Central Brazil. *J. S. Am. Earth Sci.* 11 (5), 427–438.
- Chappell, B.W., White, A.J.R., 2001. Two contrasting granite types: 25 years later. *Aust. J. Earth Sci.* 48 (4), 489–499.
- Chen, J.F., Jahn, B.M., 1998. Crustal evolution of southeastern China: Nd and Sr isotopic evidence. *Tectonophysics* 284 (1–2), 101–133.
- Chen, P.R., Kong, X.G., Wang, Y.X., Ni, Q.S., Zhang, B.T., Ling, H.F., 1999. Rb-Sr isotopic dating and significance of early Yanshanian bimodal volcanic-intrusive complex from southern Jiangxi Province, SE China. *Geol. J. China Univ.* 5, 378–382 (in Chinese with English abstract).
- Chen, B., Ma, X.H., Wang, Z.Q., 2014. Origin of the fluorine-rich highly differentiated granites from the Qianlishan composite plutons (South China) and implications for polymetallic mineralization. *J. Asian Earth Sci.* 93, 301–314.
- Collins, W.J., Beams, S.D., White, A.J.R., Chappell, B.W., 1982. Nature and origin of A-type granites with particular reference to southeastern Australia. *Contrib. Miner. Petrol.* 80 (2), 189–200.
- Douce, A.E.P., 1997. Generation of metaluminous A-type granites by low-pressure melting of calc-alkaline granitoids. *Geology* 25 (8), 743–746.
- Eby, G.N., 1992. Chemical subdivision of the a-type granitoids: petrogenetic and tectonic implications. *Geology* 20 (7), 641–644.
- Eby, G.N., Kochhar, N., 1990. Geochemistry and petrogenesis of the Malani igneous suite, North Peninsular India. *J. Geol. Soc. India* 36 (2), 109–130.
- Faure, M., Natalin, B., 1992. The geodynamic evolution of the eastern Eurasian margin in Mesozoic times. *Tectonophysics* 208 (4), 397–411.
- Fu, J.M., Ma, C.Q., Xie, C.F., Zhang, Y.M., Peng, S.B., 2004. SHRIMP U-Pb zircon dating of the Jiuyishan composite granite in Hunan and its geological significance. *Geotectonica Metallogenica* 28 (4), 370–378 (in Chinese with English abstract).
- Fu, J.M., Cheng, S.B., Lu, Y.Y., Wu, S.C., Ma, L.Y., Chen, X.Q., 2012. Geochronology of the greisen-quartz-vein type tungsten-tin deposit and its host granite in Xitian, Hunan Province. *Geol. Prospect.* 48 (2), 0313–0320 (in Chinese with English abstract).
- Gilder, S.A., Keller, G.R., Luo, M., Goodell, P.C., 1991. Timing and spatial-distribution of rifting in China. *Tectonophysics* 197 (2–4), 225–243.
- Gilder, S.A., Gill, J., Coe, R.S., Zhao, X.X., Liu, Z.W., Wang, G.X., Yuan, K.R., Liu, W.L., Kuang, G.D., Wu, H.R., 1996. Isotopic and paleomagnetic constraints on the Mesozoic tectonic evolution of south China. *J. Geophys. Res.–Solid Earth* 101 (B7), 16137–16154.
- Green, T.H., 1995. Significance of Nb/Ta as an indicator of geochemical processes in the crust–mantle system. *Chem. Geol.* 120 (3–4), 347–359.
- Haapala, I., Lukkari, S., 2005. Petrological and geochemical evolution of the Kymi stock, a topaz granite cupola within the Viborg rapakivi batholith, Finland. *Lithos* 80 (1–4), 347–362.
- Han, B.F., Wang, S.G., Jahn, B.M., Hong, D.W., Kagami, H., Sun, Y.L., 1997. Depleted-mantle source for the Ulungur River A-type granites from North Xinjiang, China: geochemistry and Nd-Sr isotopic evidence, and implications for Phanerozoic crustal growth. *Chem. Geol.* 138, 135–159.
- Heinrich, C.A., 1990. The chemistry of hydrothermal tin-(tungsten) ore deposition. *Econ. Geol.* 85 (3), 457–481.
- Hsü, K.J., Li, J.L., Chen, H.H., Wang, Q.C., Sun, S., Sengor, A.M.C., 1990. Tectonics of South China: key to understanding West Pacific geology. *Tectonophysics* 183 (1–4), 9–39.
- Huang, X.L., Xu, Y.G., Lo, C.H., Wang, R.C., Lin, C.Y., 2007. Exsolution lamellae in a clinopyroxene megacryst aggregate from Cenozoic basalt, Leizhou Peninsula, South China: petrography and chemical evolution. *Contrib. Miner. Petrol.* 154, 691–705.
- Huang, H.Q., Li, X.H., Li, W.X., Li, Z.X., 2011. Formation of high $\delta^{18}\text{O}$ fayalite-bearing A-type granite by high temperature melting of granulitic metasedimentary rocks, southern China. *Geology* 39, 903–906.

- Huang, H.Q., Li, X.H., Li, Z.X., Li, W.X., 2013. Intralate crustal remelting as the genesis of Jurassic high-K granites in the coastal region of the Guangdong Province, SE China. *J. Asian Earth Sci.* 74, 280–302.
- Jahn, B.M., Chen, P.Y., Yen, T.P., 1976. Rb-Sr ages of granitic rocks in southeastern China and their tectonic significance. *Geol. Soc. Am. Bull.* 87 (5), 763–776.
- Jahn, B.M., Wu, F.Y., Capdevila, R., Martineau, F., Zhao, Z.H., Wang, Y.X., 2001. Highly evolved juvenile granites with tetrad REE patterns: the Woduhe and Baerzhe granites from the Great Xing'an Mountains in NE China. *Lithos* 59 (4), 171–198.
- Jiang, X.Y., Li, X.H., 2014. In situ zircon U-Pb and Hf-O isotopic results for ca. 73 Ma granite in Hainan Island: implications for the termination of an Andean-type active continental margin in southeast China. *J. Asian Earth Sci.* 82, 32–46.
- Jiang, Y.H., Ling, H.F., Jiang, S.Y., Fan, H.H., Shen, W.Z., Ni, P., 2005. Petrogenesis of a Late Jurassic peraluminous volcanic complex and its high-Mg, potassic, quenched enclaves at Xiangshan, southeast China. *J. Petrol.* 46 (6), 1121–1154.
- Jiang, Y.H., Jiang, S.Y., Zhao, K.D., Ling, H.F., 2006. Petrogenesis of Late Jurassic Qianlshan granites and mafic dykes, Southeast China: implications for a back-arc extension setting. *Geol. Mag.* 143 (4), 457–474.
- Jiang, Y.H., Jiang, S.Y., Dai, B.Z., Liao, S.Y., Zhao, K.D., Ling, H.F., 2009. Middle to late Jurassic felsic and mafic magmatism in southern Hunan province, southeast China: implications for a continental arc to rifting. *Lithos* 107 (3–4), 185–204.
- Jiang, Y.H., Zhao, P., Zhou, Q., Liao, S.Y., Jin, G.D., 2011. Petrogenesis and tectonic implications of Early Cretaceous S- and A-type granites in the northwest of the Gan-Hang rift, SE China. *Lithos* 121 (1–4), 55–73.
- King, P.L., White, A.J.R., Chappell, B.W., Allen, C.M., 1997. Characterization and origin of aluminous A-type granites from the Lachlan Fold Belt, Southeastern Australia. *J. Petrol.* 38 (3), 371–391.
- Lapierre, H., Jahn, B.M., Charvet, J., Yu, Y.W., 1997. Mesozoic felsic arc magmatism and continental olivine tholeiites in Zhejiang province and their relationship with the tectonic activity in southeastern China. *Tectonophysics* 274 (4), 321–338.
- Lehmann, B., Harmanto, 1990. Large-scale tin depletion in the Tanjungpandan tin granite, Belitung Island, Indonesia. *Econ. Geol. Bull. Soc. Econ. Geol.* 85 (1), 99–111.
- Li, X.H., 1991. Geochronology of wanyangshan-zhuguangshan granitoid batholith: implication for the crust development. *Sci. in China (Series B)* 34 (5), 620–629.
- Li, X.H., McCulloch, M.T., 1996. Secular variation in the Nd isotopic composition of Neoproterozoic sediments from the southern margin of the Yangtze Block: evidence for a proterozoic continental collision in southeast China. *Precambr. Res.* 76 (1–2), 67–76.
- Li, X.H., McCulloch, M.T., 1998. Geochemical characteristics of Cretaceous mafic dikes from Northern Guangdong, SE China: age, origin and tectonic significance, mantle dynamics and plate interactions in East Asia. *Am. Geophys. Union*, 405–419.
- Li, X.H., Chung, S.L., Zhou, H.W., Lo, C.H., Liu, Y., Chen, C.H., 2004a. Jurassic intralate magmatism in southern Hunan-eastern Guangxi: 40Ar/39Ar dating, geochemistry, Sr-Nd isotopes and implications for the tectonic evolution of SE China. *Geol. Soc. Lond., Spec. Pub.* 226 (1), 193–215.
- Li, X.H., Liu, D.Y., Sun, M., Li, W.X., Liang, X.R., Liu, Y., 2004b. Precise Sm-Nd and U-Pb isotopic dating of the supergiant Shizhuoyuan polymetallic deposit and its host granite, SE China. *Geol. Mag.* 141 (2), 225–231.
- Li, X.H., Li, Z.X., Li, W.X., Wang, Y., 2006a. Initiation of the Indosinian Orogeny in South China: evidence for a Permian Magmatic Arc on Hainan Island. *J. Geol.* 114, 341–353.
- Li, X.H., Li, Z.X., Wingate, M.T.D., Chung, S.L., Liu, Y., Lin, G.C., Li, W.X., 2006b. Geochemistry of the 755 Ma Mundine Well dyke swarm, northwestern Australia: part of a Neoproterozoic mantle superplume beneath Rodinia? *Precambr. Res.* 146 (1–2), 1–15.
- Li, X.H., Li, Z.X., Li, W.X., Liu, Y., Yuan, C., Wei, G.J., Qi, C.S., 2007a. U-Pb zircon, geochemical and Sr-Nd-Hf isotopic constraints on age and origin of Jurassic I- and A-type granites from central Guangdong, SE China: A major igneous event in response to foundering of a subducted flat-slab? *Lithos* 96 (1–2), 186–204.
- Li, Z.X., Wartho, J., Occhipinti, S.A., Zhang, C.L., Li, X.H., Wang, J., Bao, C.M., 2007b. Early history of the eastern Sibao Orogen (South China) during the assembly of Rodinia: New mica 40Ar/39Ar dating and SHRIMP U-Pb detrital zircon provenance constraints. *Precambr. Res.* 159, 79–94.
- Li, X.H., Li, W.X., Li, Z.X., 2007c. On the genetic classification and tectonic implications of the Early Yanshanian granitoids in the Nanling Range, South China. *Chin. Sci. Bull.* 52 (14), 1873–1885.
- Li, X.H., Li, W.X., Li, Z.X., Lo, C.H., Wang, J., Ye, M.F., Yang, Y.H., 2009. Amalgamation between the Yangtze and Cathaysia Blocks in South China: constraints from SHRIMP U-Pb zircon ages, geochemistry and Nd-Hf isotopes of the Shuangxiwu volcanic rocks. *Precambr. Res.* 174, 117–128.
- Li, X.H., Li, W.X., Wang, X.C., Li, Q.L., Liu, Y., Tang, G.Q., Gao, Y.Y., Wu, F.Y., 2010a. SIMS U-Pb zircon geochronology of porphyry Cu-Au-(Mo) deposits in the Yangtze River Metallogenic Belt, eastern China: magmatic response to early Cretaceous lithospheric extension. *Lithos* 119, 427–438.
- Li, X.M., Hu, R.Z., Bi, X.W., Peng, J.T., 2010b. Geochemistry and tin-metallogenetic potential for Qitianling granite mass in Southern Hunan. *J. Jilin Univ. (Earth Sci. Ed.)* 40 (1), 80–92 (in Chinese with English abstract).
- Li, X.H., Long, W.G., Li, Q.L., Liu, Y., Zheng, Y.F., Yang, Y.H., Chamberlain, K.R., Wan, D.F., Guo, C.H., Wang, X.C., Tao, H., 2010c. Penglai zircon megacryst: a potential new working reference for microbeam analysis of Hf-O isotopes and U-Pb age. *Geostand. Geanal. Res.* 34, 117–134.
- Li, Z.X., Li, X.H., Chung, S.L., Lo, C.H., Xu, X.S., Li, W.X., 2012. Magmatic switch-on and switch-off along the South China continental margin since the Permian: transition from an Andean-type to a Western Pacific-type plate boundary. *Tectonophysics* 532–535, 271–290.
- Liu, G.Q., Wu, S.C., Du, A.D., Fu, J.M., Yang, X.J., Tang, Z.H., Wei, J.Q., 2008. Metallogenetic ages of the Xitian tungsten-tin deposit, eastern Hunan Province. *Geotectonica Metallogenica* 32 (1), 63–71 (in Chinese with English abstract).
- Liu, Y.S., Hu, Z.C., Zong, K.Q., Gao, C.G., Gao, S., Xu, J.A., Chen, H.H., 2010. Reappraisal and refinement of zircon U-Pb isotope and trace element analyses by LA-ICP-MS. *Chin. Sci. Bull.* 55 (15), 1535–1546.
- Loiselle, M.C., Wones, D.R., 1979. Characteristics of anorogenic granites. *Geol. Soc. Am. Abstr. Programs* 11, 468.
- Lu, Y.F., Ma, L.Y., Qu, W.J., Mei, Y.P., Chen, X.Q., 2006. U-Pb and Re-Os isotope geochronology of Baoshan Cu-Mo polymetallic ore deposit in Hunan province. *Acta Petrol. Sinica* 22 (10), 2483–2492.
- Ludwig, K.R., 2001. Users manual for Isoplot/Ex rev. 2.49. Berkeley Geochronology Centre Special Publication.: No. 1a, 56pp.
- Lv, K., Wang, Y., Xiao, J., 2011. Geochemistry characteristics of Xihuashan granite and structural environment discussion. *J. East China Inst. Technol.* 34 (2), 117–128 (in Chinese with English abstract).
- Ma, L.Y., Lu, Y.F., Mei, Y.P., Chen, X.Q., 2006. Zircon SHRIMP U-Pb dating of granodiorite from Shuikuoshan ore-field, Hunan province and its geological significance. *Acta Petrol. Sinica* 22 (10), 2475–2482.
- Ma, L.Y., Fu, J.M., Wu, S.C., Xu, D.M., Yang, X.J., 2008. 40Ar/39Ar isotopic dating of the Longshang tin-polymetallic deposit, Xitian or field, eastern Hunan. *Geol. China* 35 (4), 706–713 (in Chinese with English abstract).
- Mao, J.W., Xie, G.Q., Cheng, Y.B., Chen, Y.C., 2009. Mineral deposit models of Mesozoic ore deposits in South China. *Geol. Rev.* 55 (3), 347–354 (in Chinese with English abstract).
- Martin, R.F., 2006. A-type granites of crustal origin ultimately result from open-system fenitization-type reactions in an extensional environment. *Lithos* 91, 125–136.
- Martin, H., Bonin, B., Capdevila, R., Jahn, B.M., Lameyre, J., Wang, Y., 1994. The Kuiqi Peralkaline granitic complex (SE China): petrology and geochemistry. *J. Petrol.* 35 (4), 983–1015.
- Maruyama, S., Seno, T., 1986. Orogeny and relative plate motions: example of the Japanese Islands. *Tectonophysics* 127 (3–4), 305–329.
- Meng, L.F., Li, Z.X., Chen, H.L., Li, X.H., Wang, X.C., 2012. Geochronological and geochemical results from Mesozoic basalts in southern South China Block support the flat-slab subduction model. *Lithos* 132–133, 127–140.
- Monecke, T., Kempe, U., Monecke, J., Sala, M., Wolf, D., 2002. Tetrad effect in rare earth element distribution patterns: a method of quantification with application to rock and mineral samples from granite-related rare metal deposits. *Geochim. Cosmochim. Acta* 66, 1185–1196.
- Pearce, J.A., Harris, N.B.W., Tindle, A.G., 1984. Trace-element discrimination diagrams for the tectonic interpretation of granitic-rocks. *J. Petrol.* 25 (4), 956–983.
- Peccerillo, A., Taylor, S.R., 1976. Geochemistry of Eocene calc-alkaline volcanic rocks from Kastamonu area, Northern Turkey. *Contrib. Miner. Petrol.* 58 (1), 63–81.
- Poitrasson, F., Duthou, J.L., Pin, C., 1995. The relationship between petrology and Nd isotopes as evidence for contrasting anorogenic granite genesis: example of the Corsican Province (Se France). *J. Petrol.* 36 (5), 1251–1274.
- Scherer, E., Munker, C., Mezger, K., 2001. Calibration of the lutetium-hafnium clock. *Science* 293 (5530), 683–687.
- Shen, W.Z., Xu, S.J., Wang, Y.X., Yang, J.D., 1994. Research of the Nd-Sr isotopic composition of Xihuashan granite. *Chin. Sci. Bull.* 39 (2), 154–156 (in Chinese with English abstract).
- Skjerlie, K.P., Johnston, A.D., 1993. Fluid-absent melting behaviour of a F-rich tonalite gneiss at mid-crustal pressures: implications for the generation of anorogenic granites. *J. Petrol.* 34, 785–815.
- Su, Y.P., Tang, H.F., Sylvester, P.J., Liu, C.Q., Qu, W.J., Hou, G.S., Cong, F., 2007. Petrogenesis of Karamaili alkaline A-type granites from East Junggar, Xinjiang (NW China) and their relationship with tin mineralization. *Geochim. J.* 41, 341–357.
- Sun, S.S., McDonough, W.F., 1989. Chemical and isotopic systematics of oceanic basalts: implications for mantle composition and processes. *Geol. Soc. Lond. Spec. Publ.* 42 (1), 313–345.
- Sun, F., Xu, X., Zou, H., Xia, Y., 2015. Petrogenesis and magmatic evolution of ~130 Ma A-type granites in Southeast China. *J. Asian Earth Sci.* 98, 209–224.
- Tanelli, G., 1982. Geological setting, mineralogy and genesis of tungsten mineralization in Dayu District, Jiangxi (Peoples-Republic-of-China): an outline. *Miner. Deposita* 17 (2), 279–294.
- Tatsumi, Y., Egging, S., 1995. Subduction Zone Magmatism. Blackwell Science, New York.
- Tu, X.L., Zhang, H., Deng, W.F., Ling, M.X., Liang, H.Y., Liu, Y., Sun, W.D., 2011. Application of resolution laser ablation ICPMS in trace element analyses. *Geochimica* 40, 83–98 (in Chinese with English abstract).
- Turner, S.P., Foden, J.D., Morrison, R.S., 1992. Derivation of some a-type magmas by fractionation of basaltic magma: an example from the Padthaway Ridge, South Australia. *Lithos* 28 (2), 151–179.
- Wang, Y.J., Fan, W.M., Guo, F., 2003. Geochemistry of early Mesozoic potassium-rich diorites-granodiorites in southeastern Hunan Province, South China: petrogenesis and tectonic implications. *Geochem. J.* 37 (4), 427–448.
- Wang, Y.J., Fan, W.M., Peng, T.P., Guo, F., 2004a. Early Mesozoic OIB-type alkaline basalts in central Jiangxi Province and its tectonic implication. *Geochimica* 33, 109–117 (in Chinese with English abstract).

- Wang, Q., Zhao, Z.H., Jian, P., Xu, J.F., Bao, Z.W., Ma, J.L., 2004b. SHRIMP zircon geochronology and Nd-Sr isotopic geochemistry of the Dexing granodiorite porphyries. *Acta Petrol. Sinica* 20 (2), 315–324.
- Wang, Y.J., Fan, W.M., Peng, T.P., Guo, F., 2005. Elemental and Sr-Nd isotopic systematics of the early Mesozoic volcanic sequence in southern Jiangxi Province, South China: petrogenesis and tectonic implications. *Int. J. Earth Sci.* 94 (1), 53–65.
- Wang, X.X., Wang, T., Zhang, C.L., 2013. Neoproterozoic, Paleozoic, and Mesozoic granitoid magmatism in the Qinling Orogen, China: constraints on orogenic process. *J. Asian Earth Sci.* 72, 129–151.
- Whalen, J.B., Currie, K.L., Chappell, B.W., 1987. A-type granites: geochemical characteristics, discrimination and petrogenesis. *Contrib. Miner. Petrol.* 95 (4), 407–419.
- Williams, I.S., 1992. Some observations on the use of zircon U-Pb geochronology in the study of granitic-rocks. *Trans. Roy. Soc. Edin. – Earth Sci.* 83, 447–458.
- Wong, J., Sun, M., Xing, G.F., Li, X.H., Zhao, G.C., Wong, K., Yuan, C., Xia, X.P., Li, L.M., Wu, F.Y., 2009. Geochemical and zircon U-Pb and Hf isotopic study of the Baijuhuajian metaluminous A-type granite: extension at 125–100 Ma and its tectonic significance for South China. *Lithos* 112 (3–4), 289–305.
- Wu, F.Y., Yang, Y.H., Xie, L.W., Yang, J.H., Xu, P., 2006. Hf isotopic compositions of the standard zircons and baddeleyites used in U-Pb geochronology. *Chem. Geol.* 234 (1–2), 105–126.
- Wu, S.C., Long, Z.Q., Xu, H.H., Zhou, Y., Jiang, Y., Pan, C.C., 2012. Structural characteristics and prospecting significance of the Xitian tin-tungsten polymetallic deposit, Hunan Province, China. *Geotectonica Metallogenia* 36 (2), 217–226 (in Chinese with English abstract).
- Xia, S., Zhao, D., 2014. Late Mesozoic magmatic plumbing system in the onshore-offshore area of Hong Kong: insight from 3-D active-source seismic tomography. *J. Asian Earth Sci.* 96, 46–58.
- Yang, X.J., Wu, S.C., Fu, J.M., Huang, H.L., Chang, H.L., Liu, Y.H., Wei, J.Q., Liu, G.Q., Ma, L.Y., 2007. Fluid inclusion studies of Longshang tin-polymetallic deposit in Xitian ore field, eastern Hunan Province. *Miner Deposits* 26 (5), 501–511 (in Chinese with English abstract).
- Yang, S.Y., Jiang, S.Y., Jiang, Y.H., Zhao, K.D., Fan, H.H., 2011. Geochemical, zircon U-Pb dating and Sr-Nd-Hf isotopic constraints on the age and petrogenesis of an Early Cretaceous volcanic-intrusive complex at Xiangshan, Southeast China. *Mineral. Petrol.* 101 (1–2), 21–48.
- Yang, S.Y., Jiang, S.Y., Zhao, K.D., Jiang, Y.H., Ling, H.F., Luo, L., 2012. Geochronology, geochemistry and tectonic significance of two Early Cretaceous A-type granites in the Gan-Hang Belt, Southeast China. *Lithos* 150, 155–170.
- Yao, Y., Chen, J., Lu, J.J., Zhang, R.Q., 2013. Geochronology, Hf isotopic compositions and geochemical characteristics of Xitian A-type granite and its geological significance. *Miner. Deposits* 32 (3), 467–488 (in Chinese with English abstract).
- Ye, M.F., Li, X.H., Li, W.X., Liu, Y., Li, Z.X., 2007. SHRIMP zircon U-Pb geochronological and whole-rock geochemical evidence for an early Neoproterozoic Sibaowan magmatic arc along the southeastern margin of the Yangtze Block. *Gondwana Res.* 12, 144–156.
- Yin, Z.P., Ling, H.F., Huang, G.R., Shen, W.Z., Wang, L., 2010. Research on geochemical characteristics and genesis of Jiufeng rock mass in Northern Guangdong Province. *J. East China Inst. Technol.* 33 (1), 15–21 (in Chinese with English abstract).
- Zhang, Q., 2013. Is the Mesozoic magmatism in eastern China related to the westward subduction of the Pacific plate? *Acta Petrol. Mineral.* 32 (1), 113–128 (in Chinese with English abstract).
- Zhang, S.B., Zheng, Y.F., Wu, Y.B., Zhao, Z.F., Gao, S., Wu, F.Y., 2006. Zircon U-Pb age and Hf isotope evidence for 3.8 Ga crustal remnant and episodic reworking of Archean crust in South China. *Earth Planet. Sci. Lett.* 252 (1–2), 56–71.
- Zhang, Q., Jin, W.J., Li, C.D., 2009. Yanshanian large-scale magmatism and lithosphere thinning in Eastern China: relation to large igneous province. *Earth Sci. Front.* 16 (2), 021–051.
- Zhao, Z.H., Xiong, X.L., Han, X.D., Wang, Y.X., Wang, Q., Bao, Z.W., Jahn, B.M., 2002. Controls on the REE tetrad effect in granites: evidence from the Qianlishan and Baerzhe Granites, China. *Geochem. J.* 36, 527–543.
- Zhao, G.D., Jiang, S.Y., Liu, D.Y., 2006. SHRIMP U-Pb dating of the Furong unit of Qitangling granite from southeast Hunan province and their geological implications. *Acta Petrol. Sinica* 22 (10), 2611–2616.
- Zhao, K.D., Jiang, S.Y., Zhu, J.C., Li, L., Dai, B.Z., Jiang, Y.H., Ling, H.F., 2010. Hf isotopic composition of zircons from the Huashan-Guposhan intrusive complex and their mafic enclaves in northeastern Guangxi: implication for petrogenesis. *Chin. Sci. Bull.* 55 (6), 509–519.
- Zheng, J.P., Griffin, W.L., O'Reilly, S.Y., Zhang, M., Pearson, N., Pan, Y.M., 2006. Widespread Archean basement beneath the Yangtze craton. *Geology* 34 (6), 417–420.
- Zhou, X.M., Li, W.X., 2000. Origin of Late Mesozoic igneous rocks in Southeastern China: implications for lithosphere subduction and underplating of mafic magmas. *Tectonophysics* 326 (3–4), 269–287.
- Zhou, X.M., Sun, T., Shen, W.Z., Shu, L.S., Niu, Y.L., 2006. Petrogenesis of Mesozoic granitoids and volcanic rocks in South China: a response to tectonic evolution. *Episodes* 29 (1), 26–33.
- Zhou, Q., Jiang, Y.H., Liao, S.Y., Zhao, P., Jin, G.D., Jia, R.Y., Liu, Z., Xu, S.M., 2012a. SHRIMP zircon U-Pb dating and Hf isotope studies of the diorite porphyrite from the Dexing copper deposit. *Acta Geol. Sinica* 86 (11), 1726–1734.
- Zhou, Z.H., Mao, J.W., Lyckberg, P., 2012b. Geochronology and isotopic geochemistry of the A-type granites from the Huanggang Sn-Fe deposit, southern Great Hinggan Range, NE China: implication for their origin and tectonic setting. *J. Asian Earth Sci.* 49, 272–286.
- Zhou, Y., Liang, X.Q., Liang, X.R., Wu, S.C., Jiang, Y., Wen, S.N., Cai, Y.F., 2013. Geochronology and geochemical characteristics of the Xitian tungsten-tin-bearing A-type granite, Hunan Province, China. *Geotectonica Metallogenia* 37 (3), 511–529 (in Chinese with English abstract).
- Zhu, J.C., Xie, C.F., Zhang, P.H., Yang, C., Gu, C.Y., 2005. Niemiao and Tong'an intrusive bodies of NE Guangxi: petrology, zircon SHRIMP U-Pb geochronology and geochemistry. *Acta Petrol. Sinica* 21 (3), 665–676.
- Zhu, J.C., Zhang, P.H., Xie, C.F., Zhang, H., Yang, C., 2006a. The Huashan-Guposhan A-type granitoid belt in the western part of the Nanling Mountains: petrology, geochemistry and genetic interpretations. *Acta Geol. Sinica* 80 (4), 529–542 (in Chinese with English abstract).
- Zhu, J.C., Zhang, P.H., Xie, C.F., Zhang, H., Yang, C., 2006b. Magma mixing origin of the mafic enclaves in Lisong Granite, NE Guangxi, western Nanling Mountains. *Geochimica* 35 (5), 506–516 (in Chinese with English abstract).
- Zhu, K.Y., Li, Z.X., Xu, X.S., Wilde, S.A., 2014. A Mesozoic Andean-type orogenic cycle in southeastern China as recorded by granitoid evolution. *Am. J. Sci.* 314, 187–234.